Chapter 1

Introduction

Filters are essential components in the RF front end of wireless communication systems. Microstrip planar filters are usually preferred due to its low cost, good reliability and ease in synthesis and design. In the RF front end, a high-performance planar microwave filter is usually required to have a good attenuation level in rejection bands and a sufficiently wide upper stopband. It is particularly favorable that transmission zeros can be easily created and tuned close to passband, since one of important missions of a bandpass filter is to suppress the undesired frequency components near the passband. The creation of transmission zeros in a planar filter can be achieved by establishing proper cross couplings [1-3], tapping input/output resonators [4, 5], and employing a zero degree feed scheme [6].

In [7], $\lambda/4$ microstrip resonators are proposed to design a compact and low loss filter with elliptic function-type performance. This microstrip bandpsss filter possesses two transmission zeros at upper and lower sides of the passband. The filter design in this thesis will start with the concepts in [7]. However, it is found that strong couplings between feed lines and end resonators are required in the structure, so that a small coupling gap becomes inevitable. In addition, the size of resonators needs some adjusting to perform a flat passband.

In this thesis, uniform impedance resonators (UIRs) and stepped impedance resonators (SIRs) are employed to design a bandpass filter with an elliptic function-like response and a sharp transition band, of which the idea is achieved by locating two transmission zeros close to the passband. The basic resonators are UIRs or SIRs tapped with an open stub at its center. The length of the open stub can be trimmed to control the transmission zero at either the lower or upper side of the passband. In a cascade of such two stages, one makes a transmission zero at the lower edge of the passband and the other zero at the upper edge, then a bandpass filter with

sharp transition bands can be obtained. Both direct, or parallel-line, coupling and three-line coupling microstrip structures [8] are incorporated into the design.

Chapter 2 will give the theoretical background and some important features of the proposed circuits. Although the proposed circuits can achieve the expected performance, some undesired effects in response will occur simultaneously, such as spurious responses. We will exploit some techniques to suppress these effects. Chapter 3 will demonstrate the simulated and measured responses of the fabricated bandpass filters. Chapter 4 will draw the conclusion.

Chapter 2

The Filter Structures

In this chapter, design curves for the proposed structures of two $\lambda/4$ resonators with a tapped stub to implement the elliptic function-like response will be given. First, the property of resonators tapped with a $\lambda/4$ open stub in parallel-coupled microstrip bandpass filters is investigated. The resonance characteristics of such three-end resonator are presented and discussed. Then, the filter synthesis with a cascade of two such resonators is presented. Next, two kinds of input/output coupling structures, i.e., between feed lines and end resonators, are brought out. Finally, some design skills for improvement of filter performance are proposed.

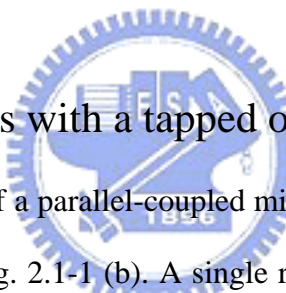## 2.1   Two $\lambda/4$ resonators with a tapped open stub

Fig. 2.1-1 (a) shows layout of a parallel-coupled microstrip line bandpass filter. Its typical passband response is shown in Fig. 2.1-1 (b). A single resonator in this bandpass filter can be considered as a $\lambda/2$ resonator or two $\lambda/4$ resonators. Our objective is to create transmission zeros near passband to implement an elliptic function-like response, as shown in Fig. 2.1-2. To generate transmission zeros, according to the method in [7], we can tap an open-end stub at the middle of the $\lambda/2$ resonator. The circuit layout of two $\lambda/4$ resonators tapped with a $\lambda/4$ open stub is shown in Fig. 2.1-3 (a), and its equivalent circuit is in Fig. 2.1-3 (b). It has been shown in [7] that two $\lambda/4$ parallel-coupled transmission-line sections can be equivalent to J-inverters, and the junction of the tapped open stub and the two $\lambda/4$ resonators works as a K-inverter. The tapped open stub has an important property that the notch frequency of the whole resonator can be adjusted by changing length of the tapped open stub, so that a transmission zero can be well controlled to locate close to the passband edge. From the equivalent circuit in Fig. 2.1-3 (b), the three-end resonator can be treated as two-pole coupled resonators. In order to simulate the

resonant properties of this structure, we apply couplings through small gaps to both ends of the resonator, as shown in Fig. 2.1-4 (a). The simulated $|S_{21}|$ response is shown in Fig. 2.1-4 (b), where two resonant frequencies: f_o and f_p and one transmission zero at f_z can be observed. Thus, that the circuit in Fig. 2.1-4 (a) is a two-pole resonator can be validated.

In Fig. 2.1-5, we plot the dependence of pole frequencies, f_o and f_p, and the transmission zero frequency f_z on stub lengths. Based on the results shown in Fig. 2.1-5, several important properties of f_z, f_o and f_p are summarized as follows. (1) The circuit has three open-circuit ends, and it has two resonant frequencies. (2) Let f_o be fixed at 2.45 GHz, the fundamental resonant frequency. One can see that it is independent of the stub length. (3) The transmission pole f_p is of course resulted from the tapped open stub, because it interacts with the resonator and hence produces an additional pole. (4) The transmission zero f_z can be located either on lower or upper side of the passband, and f_p always locates between f_o than f_z.

The properties of the two resonant frequencies have been known, but how the transmission zero occurs? The reason is given as follows. First, decompose the single section of two quarter-wave resonators with a tapped stub into several blocks of transmission line sections, as shown in Fig. 2.1-6. Then, apply the transmission (ABCD) matrix technique to calculate the transmission response S_{21} of the circuit:

$$\begin{bmatrix} A & B \\ C & D \end{bmatrix} = \begin{bmatrix} A_1 & B_1 \\ C_1 & D_1 \end{bmatrix} \begin{bmatrix} A_2 & B_2 \\ C_2 & D_2 \end{bmatrix} \begin{bmatrix} A_3 & B_3 \\ C_3 & D_3 \end{bmatrix}$$

$$= \begin{bmatrix} \cos\theta_1 & jZ_A\sin\theta_1 \\ jY_A\sin\theta_1 & \cos\theta_1 \end{bmatrix} \begin{bmatrix} 1 & 0 \\ \dfrac{j\tan\theta_2}{Z_B} & 1 \end{bmatrix} \begin{bmatrix} \cos\theta_3 & jZ_A\sin\theta_3 \\ jY_A\sin\theta_3 & \cos\theta_3 \end{bmatrix}$$

$$\Rightarrow \begin{cases} A = \cos\theta_1 \cos\theta_3 - \dfrac{Z_A}{Z_B}\sin\theta_1 \tan\theta_2 \cos\theta_3 - \sin\theta_1 \sin\theta_3 \\[2mm] B = jZ_A\left(\cos\theta_1 \sin\theta_3 + \sin\theta_1 \cos\theta_3\right) - j\dfrac{Z_A^2}{Z_B}\sin\theta_1 \tan\theta_2 \sin\theta_3 \\[2mm] C = jY_A\left(\cos\theta_1 \sin\theta_3 + \sin\theta_1 \cos\theta_3\right) - j\dfrac{1}{Z_B}\sin\theta_1 \tan\theta_2 \sin\theta_3 \\[2mm] D = \cos\theta_1 \cos\theta_3 - \dfrac{Z_A}{Z_B}\cos\theta_1 \tan\theta_2 \sin\theta_3 - \sin\theta_1 \sin\theta_3 \end{cases} \qquad (2.1)$$

The scattering parameter S_{21} and the transmission matrix are related by

$$S_{21} = \frac{2}{A + B\big/Z_0 + CZ_0 + D} \qquad (2.2)$$

If $\theta_1 + \theta_3 = \pi$, $Z_A \approx Z_B$, the scattering parameter S_{21} can be approximated as

$$S_{21} = \frac{2}{-2 + j\tan\theta_2\left[\sin\theta_1 \sin\theta_3\left(\dfrac{Z_0}{Z_B} - \dfrac{Z_A}{Z_B}\right) + \dfrac{Z_0}{Z_B}\right]} \qquad (2.3)$$

From this result, and if $Z_A \approx Z_B \approx Z_0$ hold, S_{21} can be treated as a function of θ_2, instead of θ_1 and θ_3, and the transmission zeros can be solely determined by the length of the tapped open stubs. This reflects the properties of the transmission zero in simulation shown in Fig. 2.1-5. We also investigate the effects of the tap position of the stub on the resonant properties of the resonator. In Fig. 2.1-7 (a), when shifting the tapped stub away from the center, we obtain results as shown in Fig. 2.1-7 (b), which shows that the zero is almost the same no matter where the stubs is tapped, which can also be validated by (2.1) through (2.3). Further, from the results shown in Fig. 2.1-7 (b), the insertion of the tapped stub at center of the resonator maybe the best choice, since not only the resonant frequency (i.e. the pole frequency) of the fundamental two λ/4 UIRs is not altered, but also the two resonant frequencies (i.e. poles) are

5

both at same side of the transmission zero. It is important since this eliminates the possibility of the notch appeal entering the passband. In addition, fewer couplings are required for synthesis of filter passband because the two resonant frequencies (i.e. poles) have a smaller deviation.
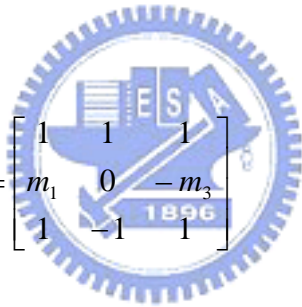
2.2   The Filter Design

The filter design method by exploiting the proposed resonator is described as follows. For a bandpass filter with an elliptic function-like response and sharp transitions at passband edges, two transmission zeros are required. Since the circuit in Fig. 2.1-4 (a) can create one transmission zero, an intuitive way is to cascade two such two-pole resonators. In the filter synthesis, according to our experience, first follow the design steps of conventional parallel-coupled bandpass filter, but passband should design with wider bandwidth than needed, Next, utilize Fig.2.1-5 to adjust the length of the tapped stub to locate two transmission zeros on both sides of the passband, change the resonator size if necessary, and then finely adjust the couplings in the structure to obtain the desired filter passband response. Since the transmission zeros have been determined by the stub length, their frequencies of transmission zeros are almost unchanged during the cascade connection of the two stages. This can greatly save time in synthesizing the filter to achieve an elliptic function-like response.

2.3   Two UIR Coupling Structures

Referring to the design steps described in Section 2.2 and [7], a two-stage UIR filter with direct coupling structure, shown in Fig. 2.3-1, can be developed. It is known that this kind of filter structure suffers from two drawbacks. One is that the strong couplings are needed between feed lines and end resonators, hence quite tight coupling gaps are inevitable, and the

other is that the dimensions of each resonators in the filter need adjusting to maintain a flat

passband response, so that the dimensions of the two quarter-wavelength UIRs with tapped

stub will be different. To solve the first problem and release the limitation of the gap size, we

apply the idea of [8], where a three-line structure is proposed. This coupling structure can

provide stronger couplings without narrow gap sizes. We call it three-line structure herein. The

circuit layout is shown in Fig. 2.3-2. For the three-line structure, there are three quasi-TEM or

dominant modes. Each mode has its modal phase constant, eigenvoltage vector, and

characteristic impedance. The inductance matrix $[L]$ and the capacitance matrix $[C]$ per unit

length for the structure can be obtained by using spectral domain approach (SDA) [10, 11].

Due to symmetry of the structure, the three-line structure can be derived from the eigenvoltage

matrix as follows.

$$[M_V] = \begin{bmatrix} 1 & 1 & 1 \\ m_1 & 0 & -m_3 \\ 1 & -1 & 1 \end{bmatrix} \tag{2.4}$$

Each vector of $[M_V]$ is the eigenvoltage vector of the matrix product of $[L][C]$. The matrix

$[M_V]$ can be used to derive the relation between port voltages and port currents which are

defined in Fig. 2.3-3 as

$$\begin{bmatrix} V_a \\ V_b \end{bmatrix} = \begin{bmatrix} Z_a & Z_b \\ Z_c & Z_d \end{bmatrix} \begin{bmatrix} I_a \\ I_b \end{bmatrix} \tag{2.5}$$

$[V_a] = [V_1 \quad V_2 \quad V_3]^T$, $[V_b] = [V_4 \quad V_5 \quad V_6]^T$, $[I_a] = [I_1 \quad I_2 \quad I_3]^T$, $[I_b] = [I_4 \quad I_5 \quad I_6]^T$ The

impedance matrix $[Z_a]$ and $[Z_b]$ can be derived as in [12]:

$$[Z_a] = [M_V]\text{diag}[-jZ_{mi}\cot\theta_i][M_V]^T \tag{2.6a}$$

$$[Z_b] = [M_V]\text{diag}[-jZ_{mi}\csc\theta_i][M_V]^T \tag{2.6b}$$

In (2.6a) and (2.6b), $\theta_i = \beta_i l$ with β_i being the phase constant of the ith mode, l being the length of the coupled section, and Z_{mi} given by

$$Z_{mi} = \frac{Z_{0i}}{m_i^2 + 2} \tag{2.7}$$

where Z_{0i} is the characteristic impedance of the ith mode. Note that in (2.7), $m_2 = 0$ should be used for mode 2. When input is connected to the second line of a symmetric three-line structure, only modes 1 and 3 will be excited, since mode 2 is an odd mode. Hence, for a six-port network in Fig. 2.3-3, if the input is connected to terminal 2, and terminal 1 and 3 are open-circuited, then the voltage and current at terminal 4 must be identical to terminal 6. We can deduce that output current is equal to $I_4 + I_6$ and the output port voltage can be V_4 or V_6. The structure terminal conditions can be written as

$$I_2 = I_i \tag{2.8a}$$

$$V_2 = V_i \tag{2.8b}$$

$$I_1 = I_3 = I_5 = 0 \tag{2.8c}$$

$$I_4 + I_6 = I_o \tag{2.8d}$$

$$V_4 = V_6 = V_o \tag{2.8e}$$

The network in Fig. 2.3-3 thus becomes a two-port. The approximations in [12] are used to establish the equivalence between the coupled section in Fig. 2.3-3 and the admittance inverter circuits in Fig. 2.3-4 (a) and Fig. 2.3-4 (b). Assume that three modal phase constants of the

three-line structure are approximately the same, and let $\beta_i l = \frac{\pi}{2}$, then compare the circuits shown in Fig. 2.3-3 and Fig. 2.3-4 (a), we obtain

$$m_1 Z_{m1} - m_3 Z_{m3} = J Z_A Z_B \qquad (2.9a)$$

$$m_1^2 Z_{m1} - m_3^2 Z_{m3} = Z_A \left(J^2 Z_A Z_B + 1 \right) \qquad (2.9b)$$

$$Z_{m1} - Z_{m3} = Z_B \left(J^2 Z_A Z_B + 1 \right) \qquad (2.9c)$$

According to [12], we can further approximate Fig. 2.3-4 (a) to Fig. 2.3-4 (b) with $Z_0^2 = Z_A Z_B$. To meet this purpose, the product of (2.9b) and (2.9c) is reduced to following approximation:

$$m_1^2 + m_3^2 \approx 2 m_1 m_3 \qquad (2.10)$$

Then we obtain

$$m_1 Z_{m1} + m_3 Z_{m3} \approx Z_0 \left(J^2 Z_0^2 + 1 \right) \qquad (2.11)$$

From the design equations for a bandpass filter in [13], the value of JZ_0 for each admittance inverter can be determined from the values of lumped elements of the lowpass filter prototype. Once JZ_0 is determined, (2.9a) and (2.11) can be solved to determine the value of $m_1 Z_{m1}$ and $m_3 Z_{m3}$ for each coupled section. The results are

$$m_3 Z_{m3} \approx \left(\frac{Z_0}{2} \right) \left(J^2 Z_0^2 - J Z_0 + 1 \right) \qquad (2.12a)$$

$$m_1 Z_{m1} \approx \left(\frac{Z_0}{2} \right) \left(J^2 Z_0^2 + J Z_0 + 1 \right) \qquad (2.12b)$$

Compare (2.12a) and (2.12b) with the design equations of the traditional coupled-line filter in [13, (8.108)], we can easily deduce that m_1Z_{m1} and m_3Z_{m3} in three-line coupled section play the same roles as those $Z_{oe}/2$ and $Z_{oo}/2$ in a two-line coupled section. It is known that the coupling coefficient C for traditional two-line coupled section can be written as

$$C = \frac{Z_{oe}/2 - Z_{oo}/2}{Z_{oe}/2 + Z_{oo}/2} \qquad (2.13)$$

Then, the coupling coefficient K for three-line coupled section can be defined as

$$K = \frac{m_1Z_{m1} - m_3Z_{m3}}{m_1Z_{m1} + m_3Z_{m3}} \qquad (2.14)$$

Fig. 2.3-5 plots the design graphs for two-line and three-line $\lambda/4$ coupled structure and the dimension can be determined by the graphs. From the comparison of Fig. 2.3-6, we can deduce that three-line coupling structure can provide larger coupling coefficient than conventional two-line coupling structure (i.e. $K>C$) at the same line width and coupling gap width. Hence the structure of two $\lambda/4$ UIRs with a tapped stub using three-line coupling input structure can have a flatter passband response and wider passband bandwidth.

2.4   Improvement of Filter Performance

A. Stepped Impedance Resonator

A planar filter is much favorable to have a wide stopband and enough rejection level in the stopband. The presented elliptic function-like response bandpass filters synthesized by UIRs, however, show spurious responses at twice the passband frequency. In order to

overcome this problem, stepped impedance resonators (SIRs) are introduced to improve the stopband performance of the proposed filter. Fig. 2.4-1 draws the layout of a traditional SIR. According to [5], the resonant characteristics of an SIR structure can be efficiently analyzed by odd mode and even mode analysis. The odd mode is excited, as shown in Fig. 2.4-2 (a), the center of the resonator is virtually grounded called an "electric wall". We can obtain two parallel susceptances when looking into the SIR at the P-Q plane. While this resonance occurs, the overall impedance of this half SIR should be zero. Hence, from the transmission line theory, we obtain

$$(Z_{in})_{\text{odd}} = jZ_1\left(\frac{Z_1 \tan\theta_1 \tan\theta_2 - Z_2}{Z_1 \tan\theta_2 + Z_2 \tan\theta_1}\right) = 0 \qquad (2.15a)$$

There are two possible solutions to this equation

$$Z_1 \tan\theta_1 \tan\theta_2 - Z_2 = 0 \qquad (2.15b)$$

$$Z_1 \tan\theta_2 + Z_2 \tan\theta_1 = \infty \qquad (2.15c)$$

If (2.15c) is valid, it means that $\tan\theta_1$ or $\tan\theta_2$ is infinite. Thus, (2.15a) can be rewritten as

$$\lim_{\tan\theta_1 \to \infty} jZ_1 \frac{Z_1 \tan\theta_1 \tan\theta_2 - Z_2}{Z_1 \tan\theta_2 + Z_2 \tan\theta_1} = jZ_1 \frac{Z_1}{Z_2} \tan\theta_2 = 0 \qquad (2.15d)$$

or

$$\lim_{\tan\theta_2 \to \infty} jZ_1 \frac{Z_1 \tan\theta_1 \tan\theta_2 - Z_2}{Z_1 \tan\theta_2 + Z_2 \tan\theta_1} = jZ_1 \tan\theta_1 = 0 \qquad (2.15e)$$

Obviously, if $\tan\theta_2 = 0$, then θ_2 will be 0 or π (i.e. $\lambda/2$). The solutions are unreasonable. Similarly, if $\tan\theta_1 = 0$, then θ_1 will be 0 or π (i.e. $\lambda/2$). The solutions are also unreasonable. Hence, the reasonable solution should be (2.15b) and (2.15b) can be rewritten as

$$\tan\theta_1 = R\cot\theta_2 \qquad\qquad (2.15f)$$

where impedance ratio R is defined as Z_2/Z_1.

Following the same manner, the resonance condition for the even mode can be derived. When the even mode is excited, as shown in Fig. 2.4-2 (b), the center of the resonator is open circuit and can be treated as a "magnetic wall". When this resonance occurs, the input impedance looking into the half SIR should be infinite. Hence, from the transmission line theory, we can obtain

$$(Z_{in})_{even} = jZ_1\frac{Z_1\tan\theta_1\tan\theta_2 - Z_2}{Z_1\tan\theta_2 + Z_2\tan\theta_1} = \infty \qquad (2.16a)$$

There are two possible solutions to this equation
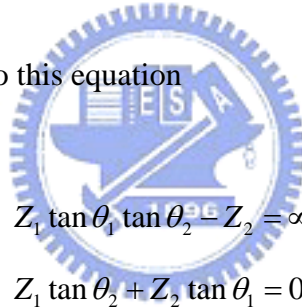
$$Z_1\tan\theta_1\tan\theta_2 - Z_2 = \infty \qquad\qquad (2.16b)$$

$$Z_1\tan\theta_2 + Z_2\tan\theta_1 = 0 \qquad\qquad (2.16c)$$

Because of the same reasons in the odd mode analysis, the reasonable solution will be (2.16c) and (2.16c) can be rewritten as

$$\cot\theta_1 = -R\cot\theta_2 \qquad\qquad (2.16d)$$

From (2.15f) and (2.16d), the resonance characteristics of an SIR can be plotted against its structure parameters as shown in Fig. 2.4-3, where the x-axis, $u = \dfrac{\theta_2}{\theta_1 + \theta_2}$, is the length ratio and those for the y-axis represent the odd mode and even mode resonant frequencies normalized to fundamental frequency of a UIR. Fig. 2.4-4 shows the graphs of the higher order

frequencies normalized to the fundamental frequency of a SIR. As shown in Fig. 2.4-4, when $R < 1$, the first higher order resonant frequency (i.e. f_2) will be pushed to higher than twice the fundamental frequency and it can be used to improve performance of the filter in the upper rejection band. At the same time, the size of the resonator can be reduced, too. According to Fig. 2.4-3 and Fig. 2.4-4, the dimension parameters of a SIR and frequencies of fundamental resonance and first higher order resonance can be determined.

B. Tapped Radial-Type Open Stub

Recall the achieved method given in Section 2.2, the creation of elliptic function-like response is by locating the zeros near the passband edges. Nevertheless, the rejection level of the side lobe is poor. It can be due to narrow bandwidth of the zero created by the tapped uniform impedance stub. According to [14], the theoretical results can show that the radial-type stub can maintain a low-impedance value in a wider frequency range than a conventional uniform impedance stub. Thus, we try to replace the uniform impedance stub with radial-type stub to acquire a better rejection level. The design methods of the planar circuit-type radial stub can be also obtained as the description in [14]. However, the design methods are complicated. When the filter is a cascade of two λ/4 resonators with a tapped radial stub, one should keep in mind two fundamental rules. One is that the radial stub will has effective size larger than the actual circuit size, and the other is that the wider the degree of the angle, the more affected the fundamental resonator. Following the design equations in [14] and the two fundamental rules described, the filter cascaded by two λ/4 resonators with a tapped radial stub can be easily synthesized.

C. Mixed Type Coupling Sturcture

After simulate and measure the two proposed coupling structures, direct coupling and three-line coupling structures discussed in Section 2.3, we find that direct coupling structure

possesses better stopband rejection level while three-line coupling structure owns flatter passband response and sharper transition on their responses. However, these second-order filters still suffer some troubles, such as quite tight coupling-gaps in direct coupling structure and poor stopband rejection level in three-line coupling structure. From Section 2.3 and measured responses, three-line coupling structure can relax the tight coupling-gap limitation, and direct coupling structure can acquire better stopband rejection level. It seems that these two structures can be a complementary of each other. Furthermore, it is known the higher the order of the filter, the larger the attenuation level in the stopband [13, Chapter 8]. Hence, the better rejection level can be obtained by employing the higher order the proposed bandpass filter. Following those concepts, we develop a star-shape bandpass filter, which consists of two sets of three-line coupling structure at the both end (i.e. input and output) stages and applying direct coupling structure at the center stage, like shown in Fig. 2.4-5. By the way, from the simulated and measured responses for the stepped impedance resonator case, the higher the spurious frequency, the better the stopband rejection level can be achieved. Consequently, the uniform impedance microstrip lines in the star-shape filter are replaced with the stepped impedance resonators so as to improve the stopband performance.

input

λ/4 λ/4 λ/4 λ/4 output
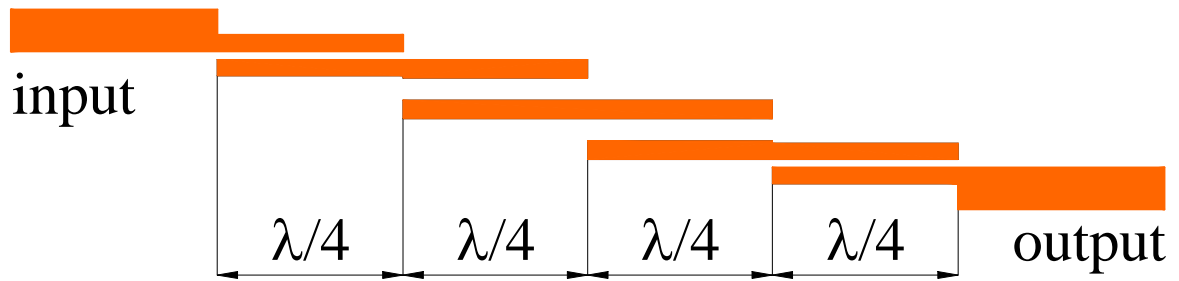
Fig. 2.1-1 (a) Circuit layout of a parallel-coupled microstrip line bandpass filter

$|S_{21}|$ (dB)

f_0

Frequency (GHz)
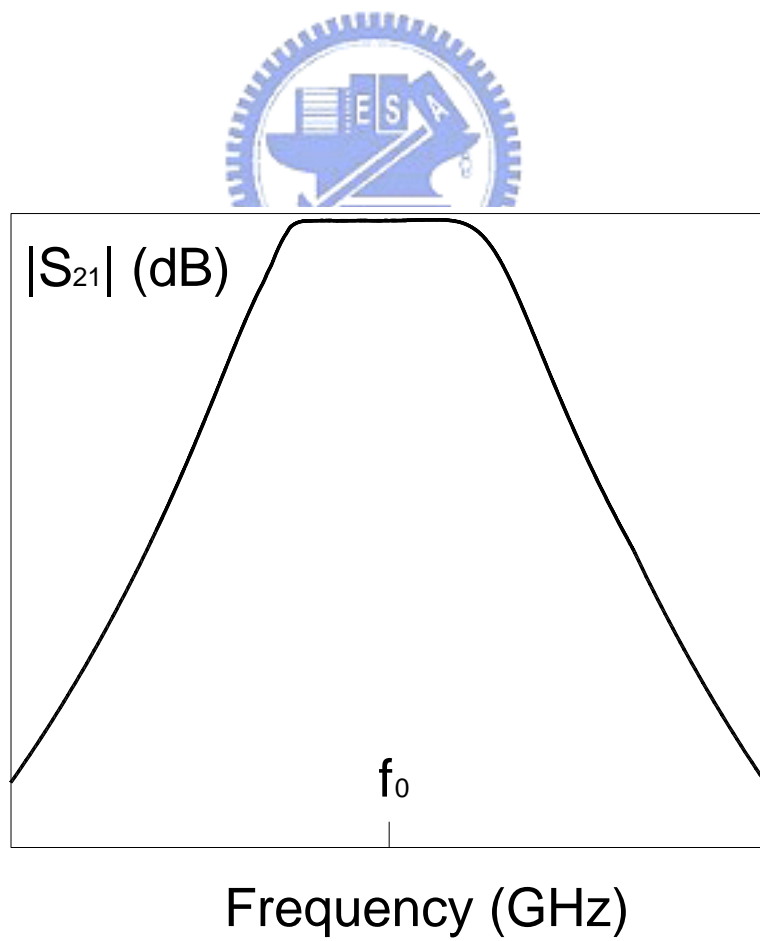
Fig. 2.1-1 (b) $|S_{21}|$ response of a parallel-coupled microstrip line bandpass filter
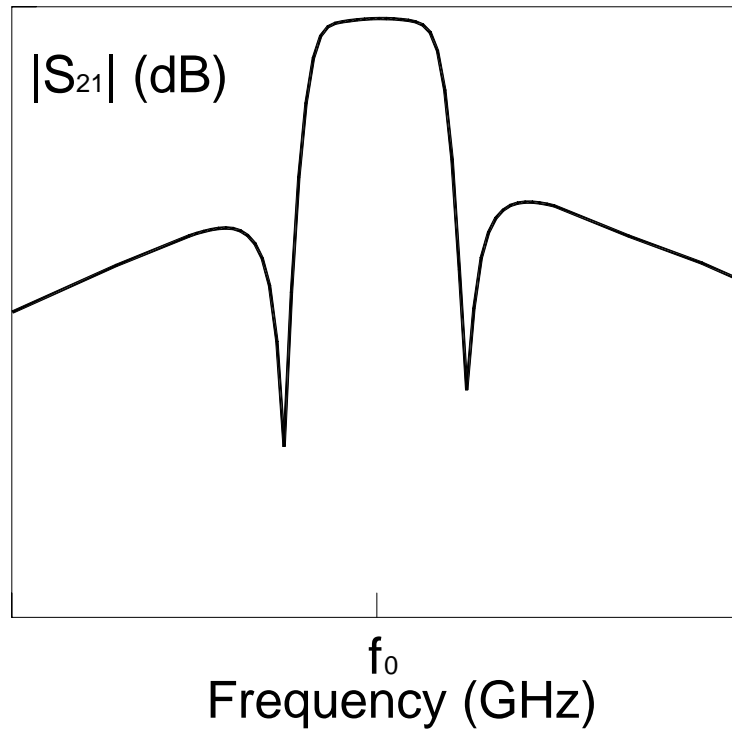
Fig. 2.1-2 Elliptic function-like response
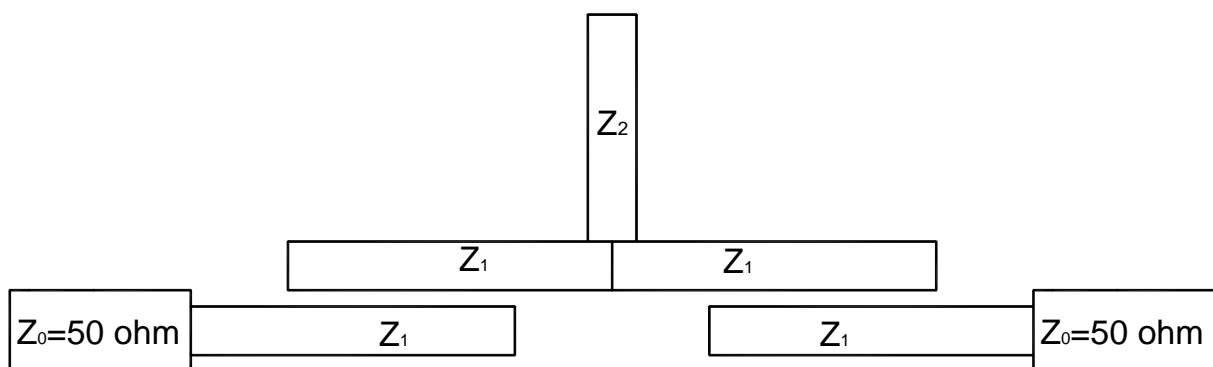
Fig. 2.1-3 (a) Circuit layout of two quarter-wavelength resonators with a tapped stub
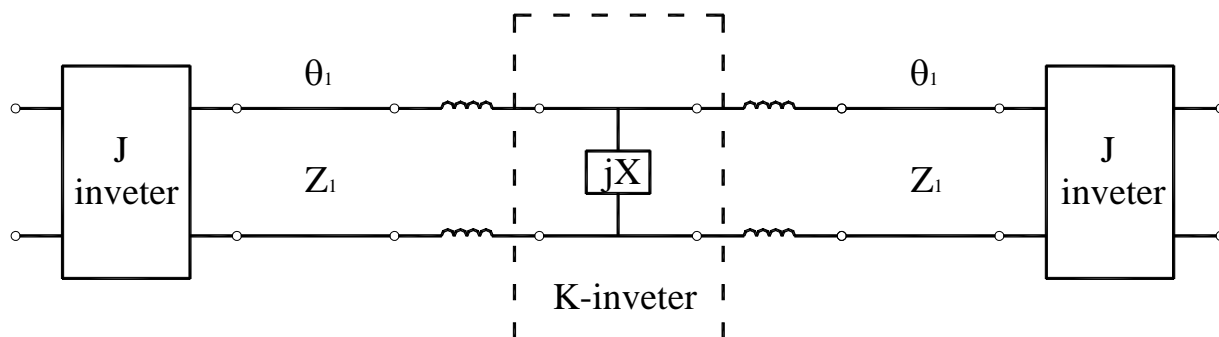
Fig. 2.1-3 (b) Equivalent circuit of two quarter-wavelength resonators with a tapped stub
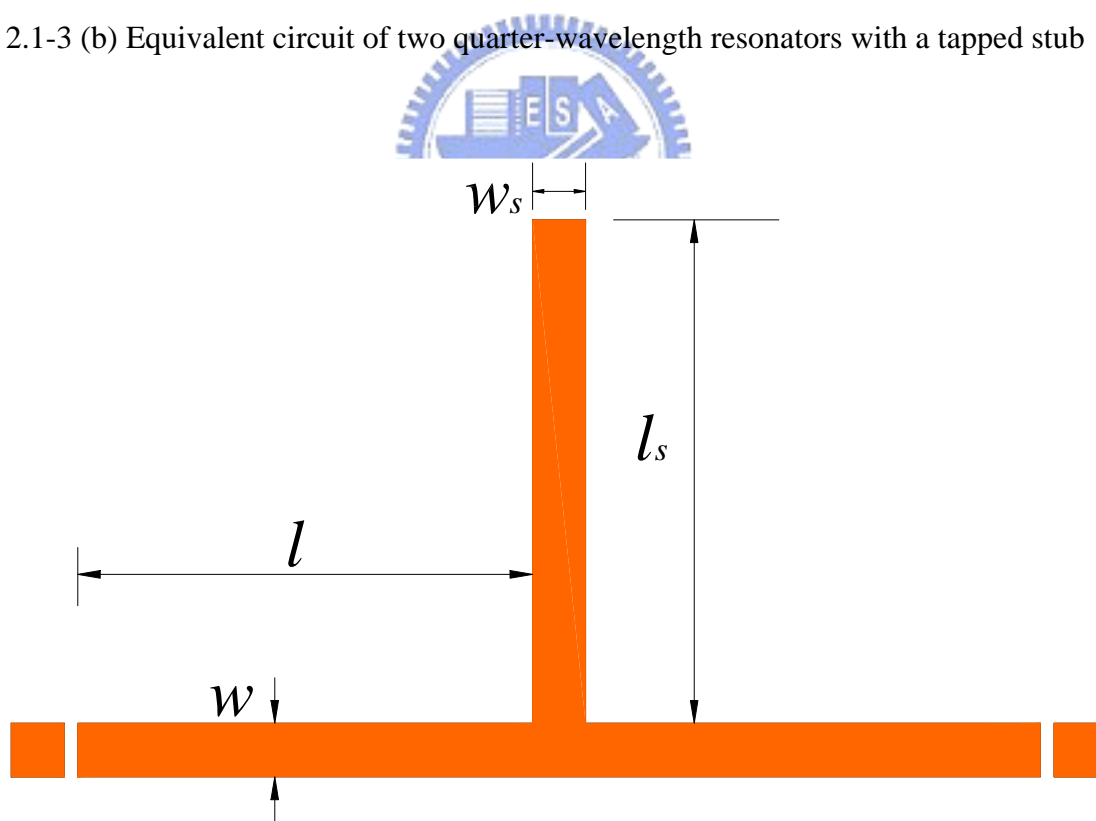
Fig. 2.1-4 (a) Circuit layout of gap-coupling test of two $\lambda/4$ UIRs with a tapped stub
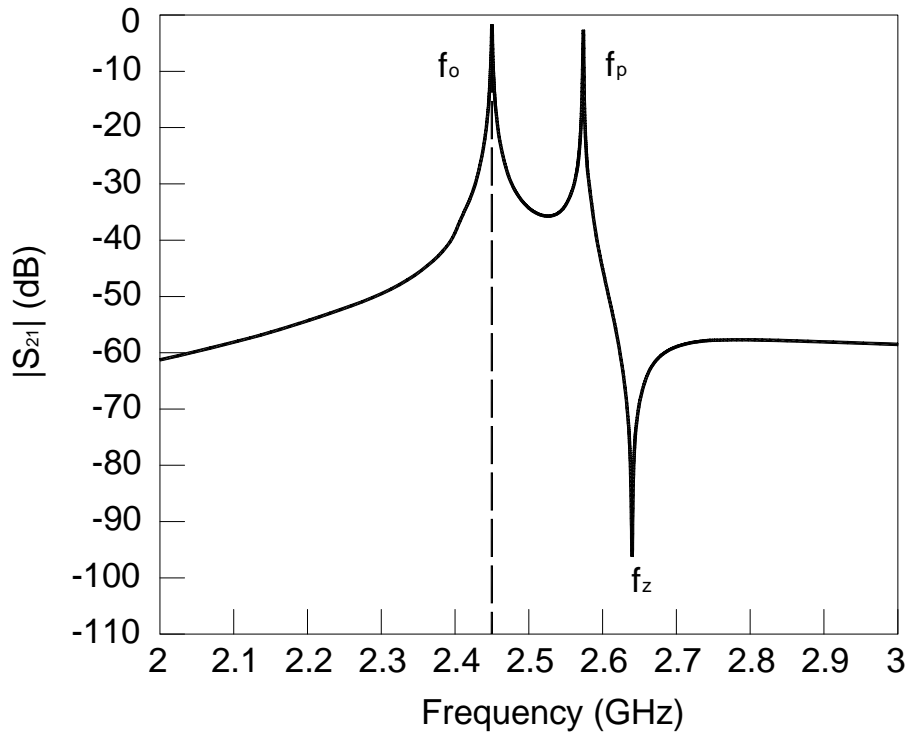
Fig. 2.1-4 (b) $|S_{21}|$ response of Fig. 2.1-4 (a)
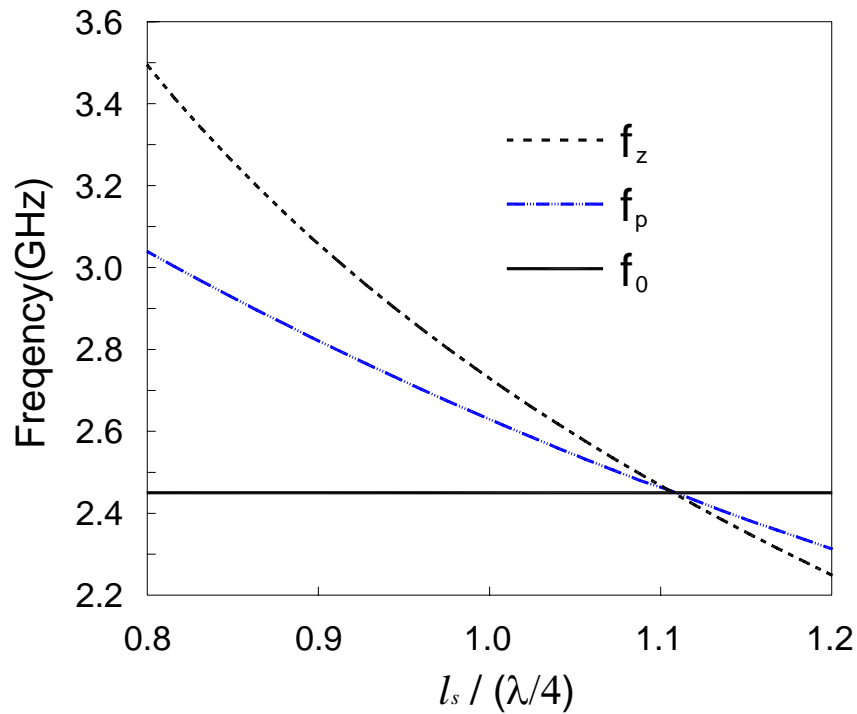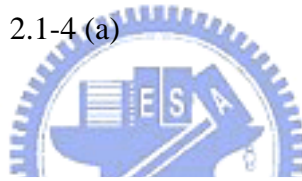
Fig. 2.1-5 Dependence of the transmission zero f_z and pole frequencies, f_o and f_p, of the UIR circuit on normalized stub length
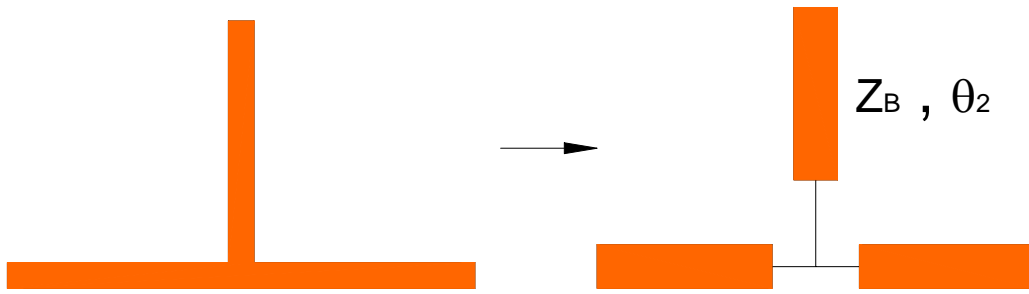
Fig. 2.1-6 Decomposition of a single section of two quarter-wavelength resonators with a tapped stub into equivalent transmission line block
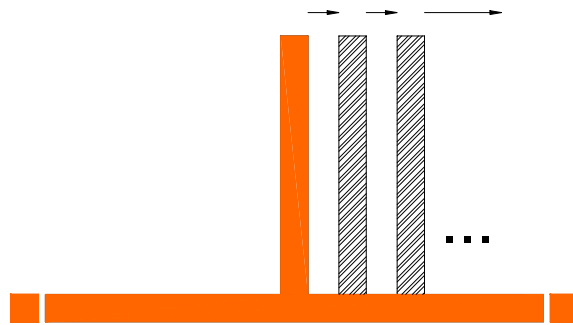
Fig.2.1-7 (a) Circuit layout of shifting the tapped stub
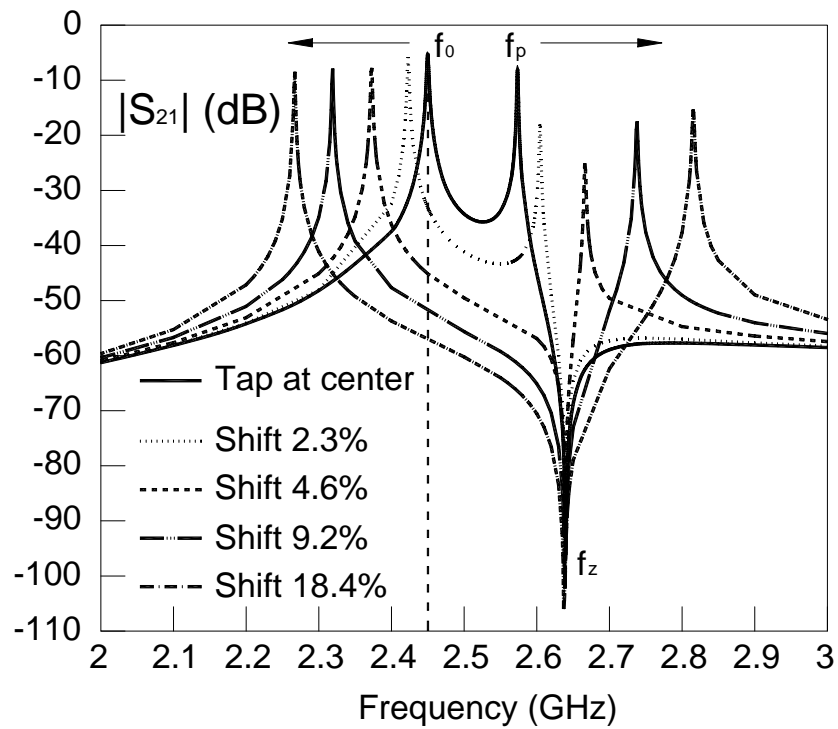
Fig 2.1-7 (b) Phenomena of shifting the tapped stub away from center of the resonator
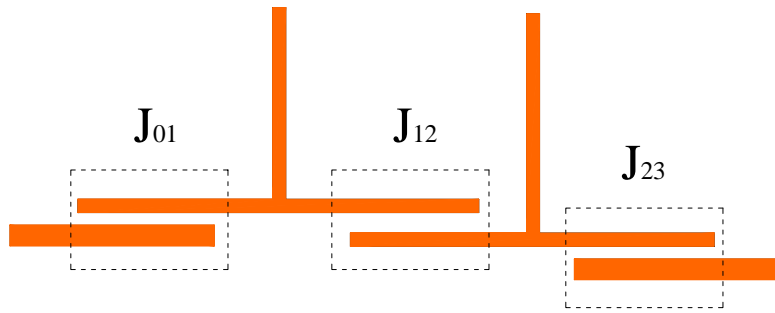
Fig 2.3-1 Circuit layout of direct coupling structure for cascading λ/4 UIRs tapped with an open stub
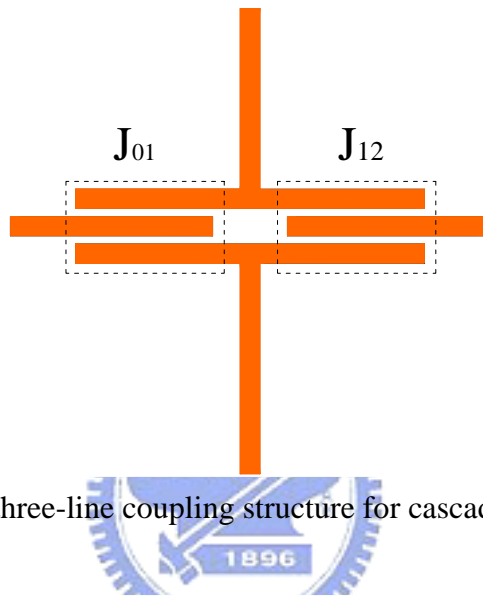
Fig. 2.3-2 Circuit layout of three-line coupling structure for cascading λ/4 UIRs tapped with an open stub
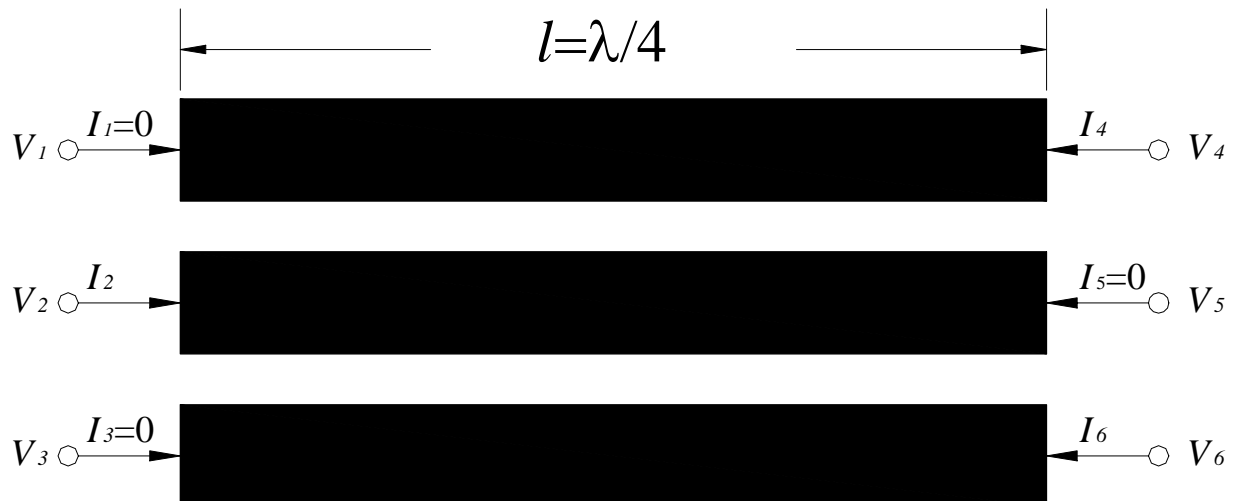
Fig. 2.3-3 Circuit layout of coupled three-line structure as a six-port network

Fig. 2.3-4 (a) Equivalent admittance inverter   (b) Further approximation of (a)
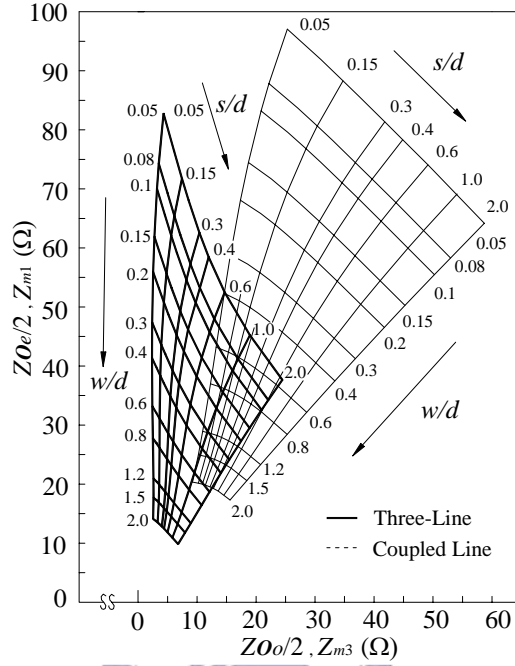
Fig. 2.3-5 Design graphs of two-line and three-line structures on a $\varepsilon_r = 10.2$ substrate
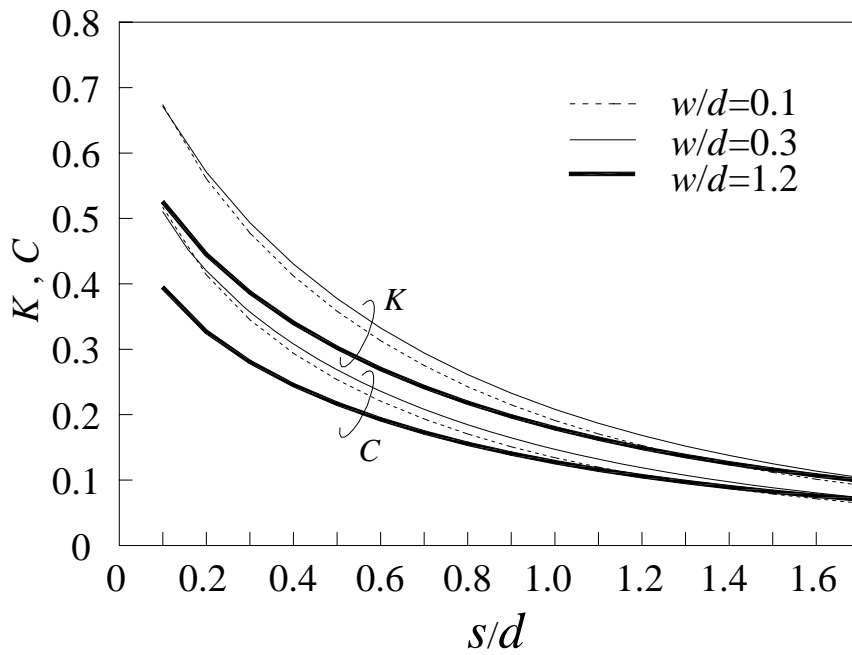
Fig. 2.3-6 Comparison of coupling coefficient of two-line and three-line quarter-wavelength coupled section on a $\varepsilon_r = 10.2$ substrate

21
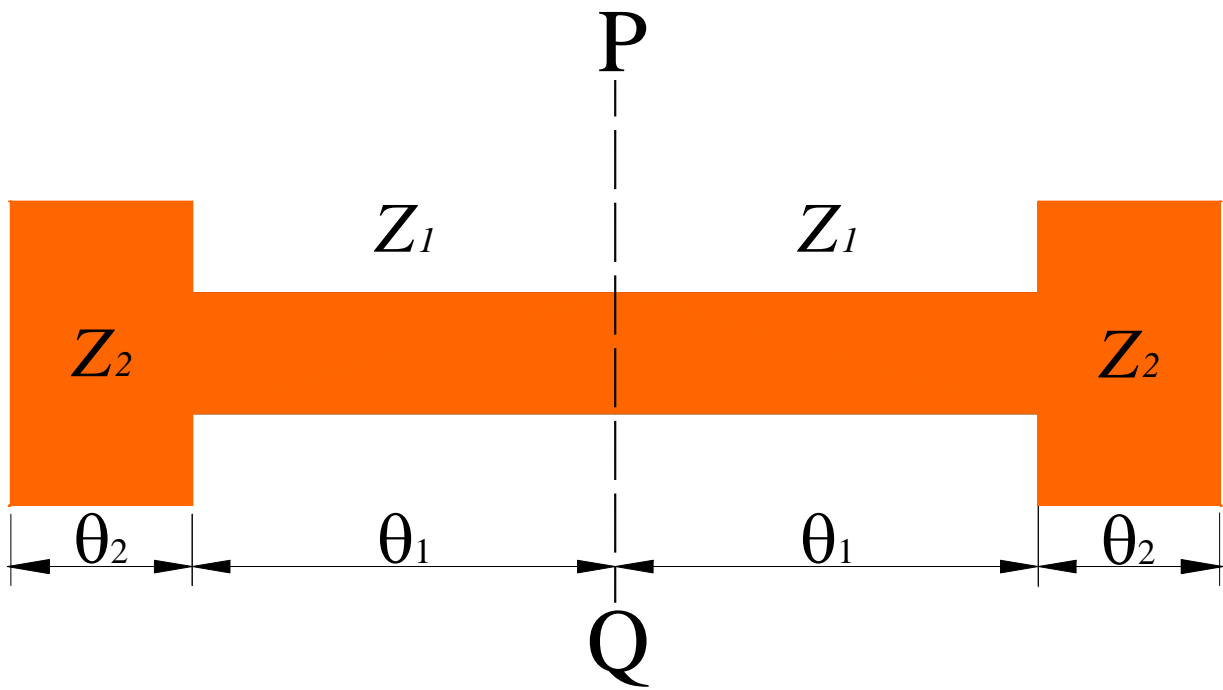
Fig. 2.4-1 Circuit layout of a SIR (stepped-impedance resonator)

electrical wall

short

$(Z_{in})_{odd}$
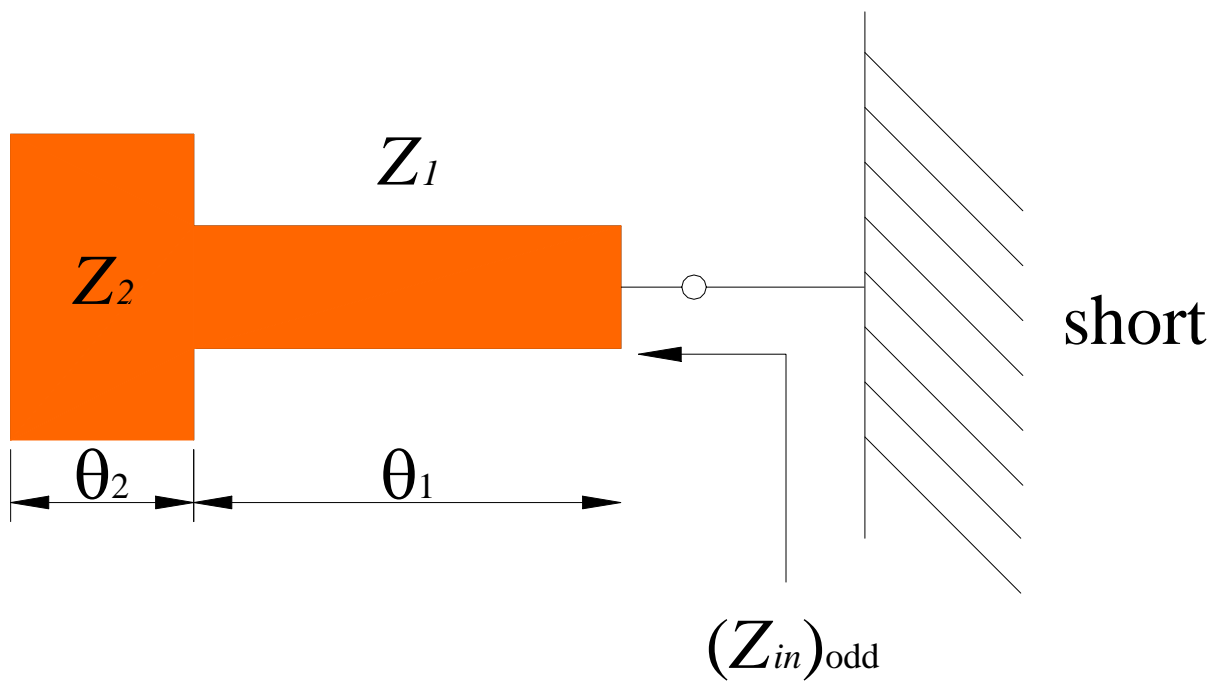
Fig. 2.4-2 (a) Odd mode excitation

magnetic wall

open

$(Z_{in})_{even}$
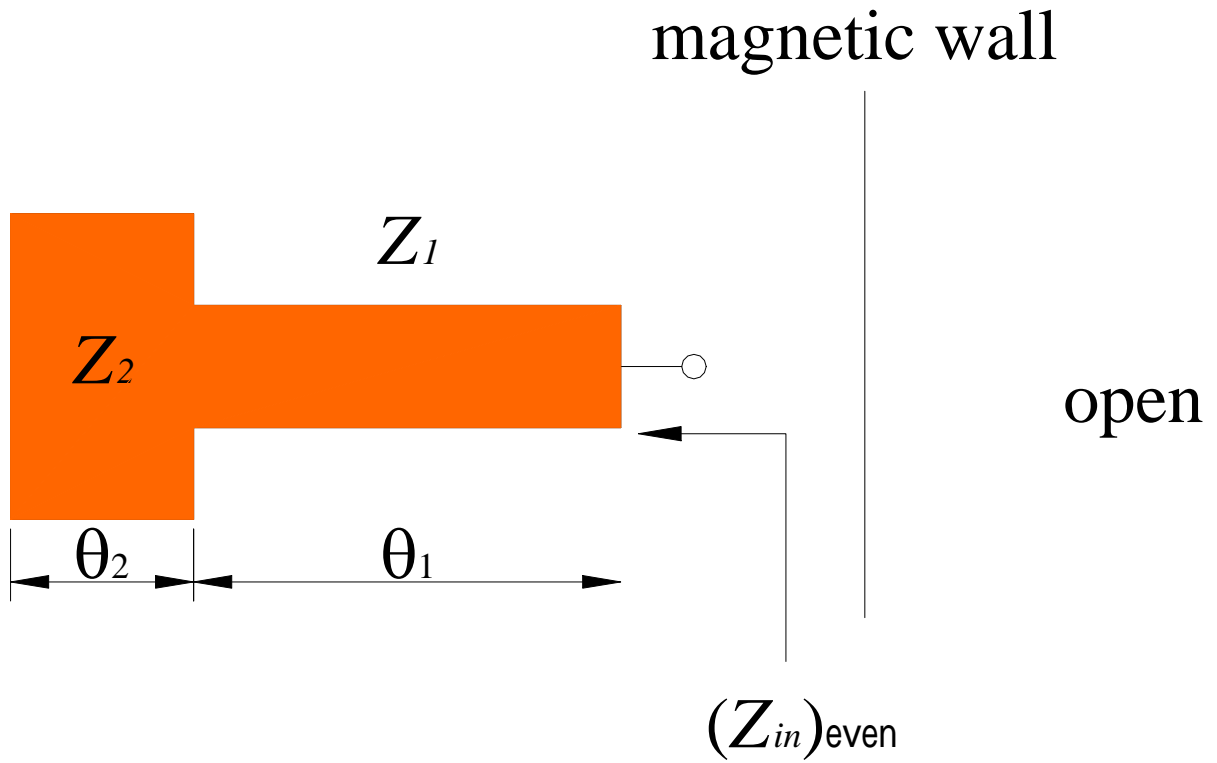
Fig. 2.4-2 (b) Even mode excitation
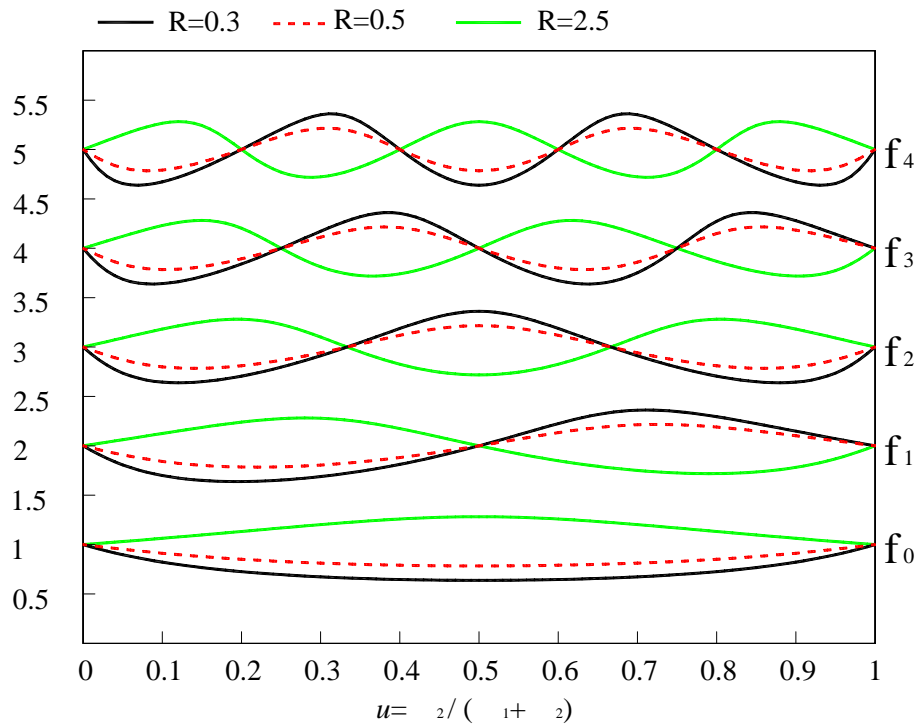
Fig. 2.4-3 Normalized resonant frequencies of a SIR
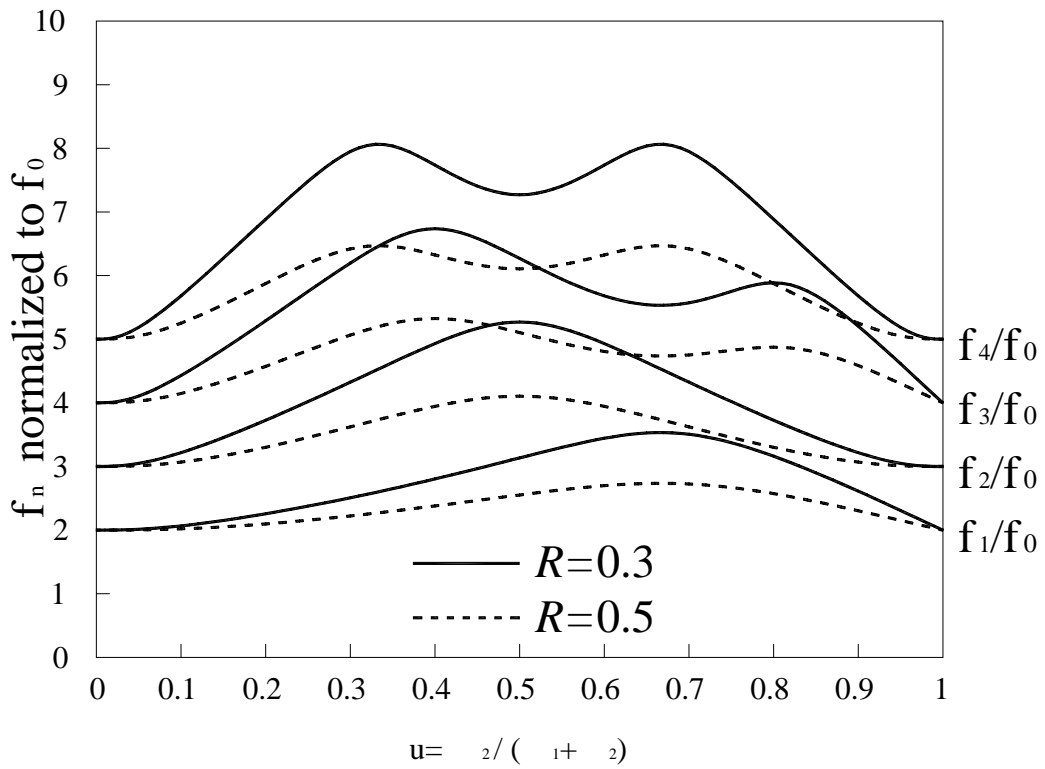
Fig. 2.4-4 Ratios of the leading four higher order resonant frequencies to the fundamental frequency of a SIR with R=0.3
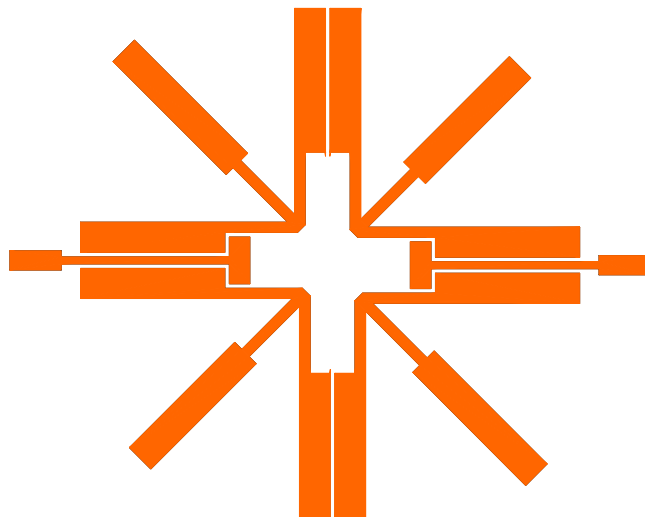
Fig. 2.4-5 Star-shape filter

Chapter 3

Simulation and Measurement Results

In this chapter, several filters with a cascade of two λ/4 resonators with a tapped stub are designed and fabricated. The full-wave simulator IE3D [9] is used for the CAD works, and an HP8720 network analyzer is used for the measurements.

Fig. 3.1-1 (a) shows the circuit layout of the filter synthesized by two λ/4 UIRs with a tapped stub using direct coupling. According to our experience, the contribution from f_p to the coupling coefficients in the filter is negligible. Thus, the synthesis of passband response can be approximated by three coefficients C_{01}, C_{12} and C_{23} determined at f_o of the main resonators. For a Butterworth response with a bandwidth $\Delta = 10\%$, $C_{01} = C_{23} = 0.30$ and $C_{12} = 0.11$. If a coupling angle of 60° is used, the gap sizes are found to be 0.25 mm and 1.2 mm for the end and middle coupled stages, respectively, for a substrate with $\varepsilon_r = 10.2$ and thickness 1.27 mm. It is found that the resonator tapped with longer stub has to be cut down by 6%, and the other one increased by 4%. Fig. 3.1-1 (b) shows the simulation and measurement results for the filter and Fig. 3.1-1 (c) shows the photo of the circuit. The actual 3-dB bandwidth of the elliptic function-like response is smaller than 10%, this is because that the zeros created by λ/4 open-end stub are forced to locate near the both passband edges. Therefore the actual bandwidth will be smaller than the designed value. The zeros are located at 2.3 and 2.6 GHz. The measured insertion loss at the center frequency is -1.5dB.

The filter can also be implemented by a three-line coupling structure in Fig. 3.1-2 (a). It is found that the size of either resonator has not to be trimmed during the synthesis and it is the benefit of exploiting the three-line coupling structure. This greatly saves effort in design such a filter. In addition, because of the stronger couplings provided by three-line coupling structure, the gap size limitation can also be released. The gap size is found to be 0.5mm, which can be

fabricated easily. Fig.3.1-2 (b) plots the simulation and measurement responses, which possess very sharp transition bands. The actual 3-dB bandwidth is also smaller than the designed value because of the zeros. Fig. 3.1-2 (c) is the photo of the circuit.

Compare the responses in Fig. 3.1-1 (b) with those in Fig. 3.1-2 (b), we can find that the three-line coupling structure possesses much sharper transition bands. The simulation and measurement responses in Fig. 3.1-1 (b) and Fig. 3.1-2 (b) present spurious responses at twice the design frequency. It degrades the attenuation level of the filter in upper rejection band. In order to improve filter performance in the stopband, we turn to design the filters with SIRs. The SIR has harmonic resonances much higher than twice the fundamental frequency if the structure parameters of the SIR (i.e. impedance ration factor and length ratio factor) can be properly determined. The two possible coupling structures for the SIR design are shown in the Fig. 3.1-3 (a) and Fig. 3.1-3 (b), where the impedance ratio R=0.3 and the length ratio $u = \dfrac{\theta_2}{\theta_1 + \theta_2} = \dfrac{2}{3}$, which will be fabricated on a substrate with $\varepsilon_r = 2.2$ and thickness 0.508 mm. Following the same design procedure in Chapter 2, Fig. 3.1-5 (a) shows the resonance characteristics of two λ/4 SIRs with a tapped open stub. The dependence of the poles and the zero are shown in Fig. 3.1-5 (b). In the direct coupling structure shown in Fig. 3.1-3 (a), the couplings between each resonator are performed by central coupled lines. Fig. 3.1-6 (a) shows the simulation and measurement responses from 2 to 3 GHz, and Fig. 3.1-6 (b) shows those from 1 to 12 GHz. The insertion loss at the center passband is -2.6dB. The filter possesses an attenuation level better than -40dB before the unwanted response goes up at 10.5 GHz. Fig. 3.1-4 (a) shows the photo of the circuit. Fig. 3.1-7 (a) plots the simulation and measurement responses of three-line coupling structure in Fig. 3.1-3 (b) from 2 to 3 GHz, the broadband responses from 1 to 10 GHz are shown in Fig. 3.1-7 (b), and Fig. 3.1-4 (b) shows the photo of the circuit. The passband insertion loss is -1.7dB at the design frequency. The spurious response goes up at 8GHz, and before this frequency the attenuation level is about -30dB.

However, from the results shown in Fig. 3.1-7 (a), we can find that the passband response is not so flat.

In order to improve flatness of the passband response, we turn to adopt a substrate with ε_r = 10.2 and thickness 1.27 mm. Based on the design procedure of the three-line coupling structure and choosing impedance ratio $R = 0.5$ and length ratio $u = \dfrac{\theta_2}{\theta_1 + \theta_2} = \dfrac{2}{3}$ for the SIRs, one can complete the design. The circuit layout is shown in Fig. 3.1-8 (a). Fig. 3.1-8 (b) and Fig. 3.1-8 (c) show the simulation and measurement responses in local and broadband views, respectively. The photo of the circuit is shown in Fig. 3.1-8 (d). An improved passband response with insertion loss -1.3dB is obtained.

However, this circuit suffers from a poor rejection level at about 8dB near the transmission zeros. It should be that the strong couplings make this undesired effect happen. To enhance the stopband performance while maintain the passband response flatness at the same time, we replace the stepped-impedance stub with a radial-type stub with the same SIR parameters: $R=0.5$ and $u = \dfrac{\theta_2}{\theta_1 + \theta_2} = \dfrac{2}{3}$, as shown in Fig. 3.1-9 (a), to widen the bandwidth of transmission zeros. The simulation and measurement results in local and broadband view are shown in Fig. 3.1-9 (b) and Fig. 3.1-9 (c), respectively. The photo of the circuit is shown in Fig. 3.1-9 (d). A flat passband response with insertion loss around -1.3dB is obtained and the 45° radial-type stub provides about 4 dB enhancement to stopband rejection level. From the results in Fig. 3.1-8 (b) and Fig. 3.1-9 (b), a good stopband rejection level and a flat passband response seem to be conflict with each other. This might be a design trade-off depending on user's demand.

Fig. 3.1-10 (a) depicts the circuit layout of mixed type (i.e. star-shape filter) bandpass filter. The resonator of two λ/4 SIRs with a tapped open stub is with size parameters of $R=0.5$ and $u = \dfrac{\theta_2}{\theta_1 + \theta_2} = \dfrac{2}{3}$. The narrowest gap width is 0.3mm, which can be fabricated out easily in general process. It should be noted that one of the four three-end resonators needs to be

shortened 0.1mm to form an acceptable passband response. The simulation and measurement results are shown in Fig. 3.1-10 (b) and Fig. 3.1-10 (c), which are the local and broadband view respectively. The passband insertion loss is about -2.5dB and the spurious response goes up at about 2.6 times the designed frequency. The worst stopband rejection level near the passband is about -28 dB, which is better than the direct coupling and three-line coupling structures synthesized by SIRs. The additional zero at about 3GHz is because the inter-stage coupling [15]. Fig. 3.1-10 (d) shows the photo of the star-shape filter.

Fig. 3.1-1 (a) Circuit layout of filter of two λ/4 UIRs with a tapped stub cascaded by direct coupling structure
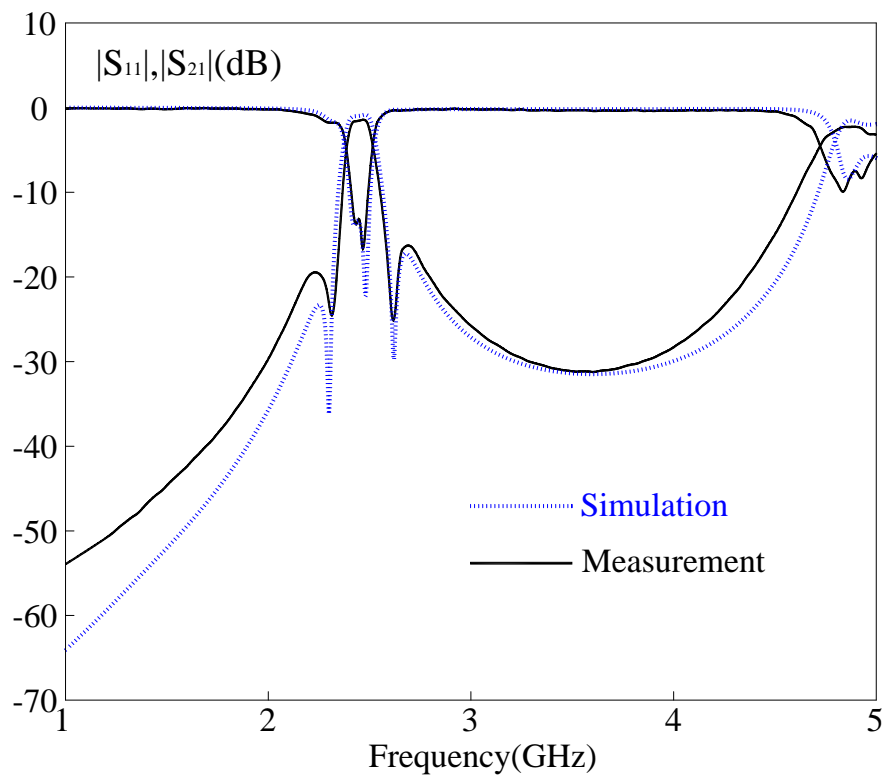
Fig. 3.1-1 (b) Simulation and measurement results of Fig 3.1-1 (a)
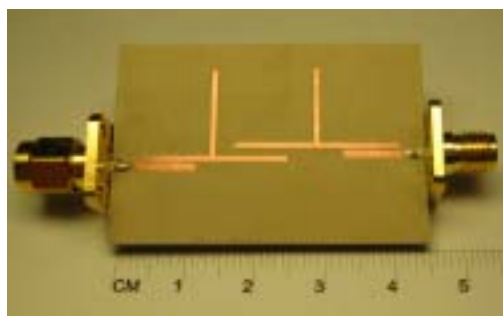
Fig. 3.1-1 (c) Photo of the circuit in Fig 3.1-1 (a)
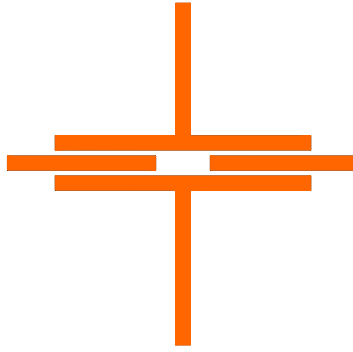
Fig. 3.1-2 (a) Circuit layout of filter of two λ/4 UIRs with a tapped stub cascaded by three-line coupling structure
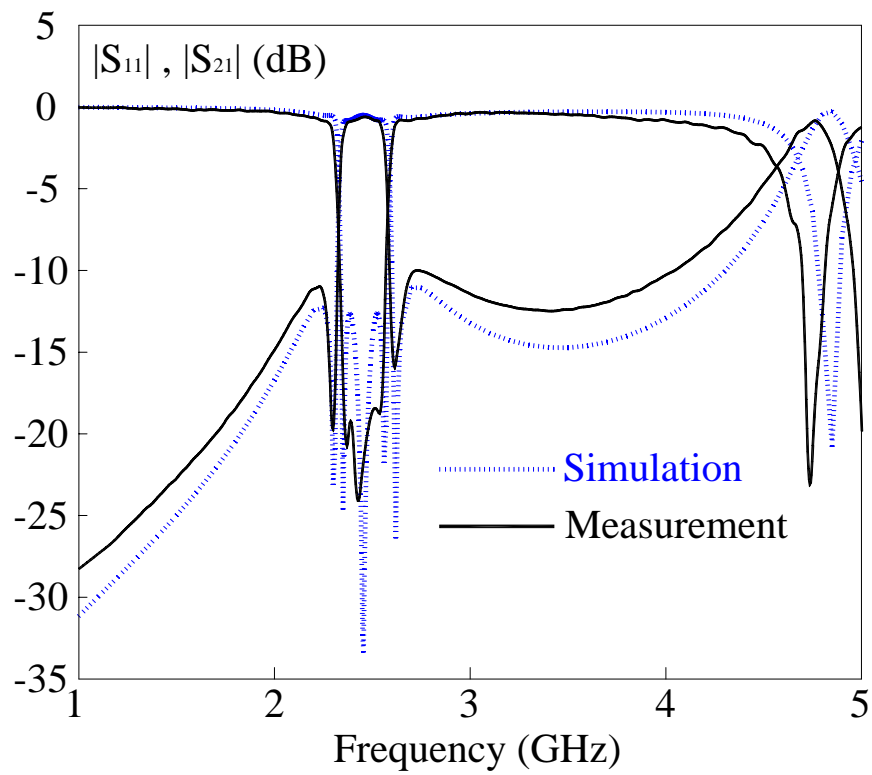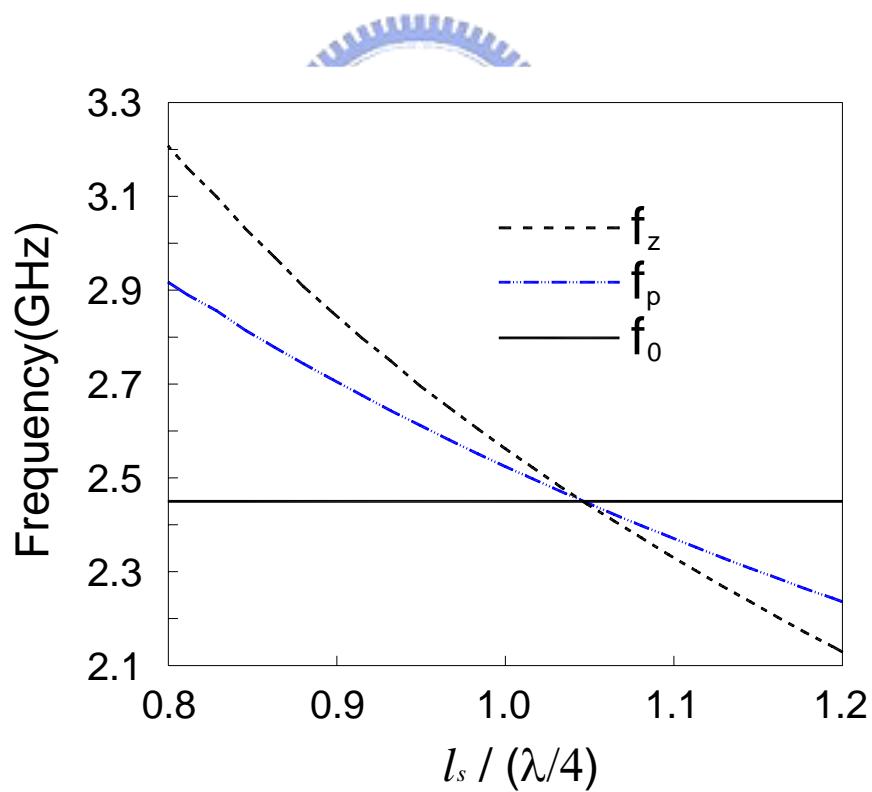

Fig. 3.1-2 (b) Simulation and measurement results of Fig 3.1-2 (a)
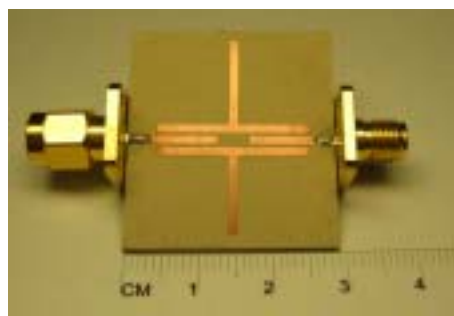
Fig. 3.1-2 (c) Photo of the circuit in Fig 3.1-2 (a)
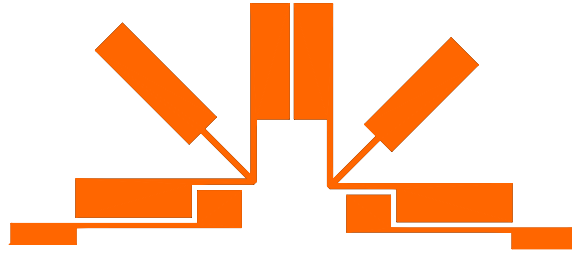
Fig. 3.1-3 (a) Circuit layout of filter of two λ/4 SIRs with a tapped stub cascaded by direct coupling structure
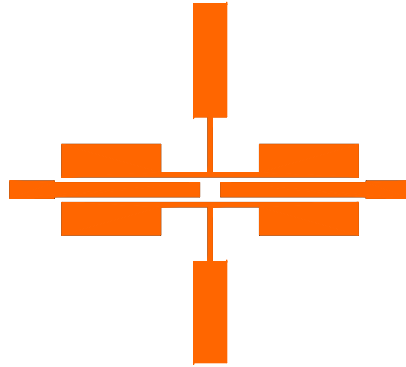
Fig. 3.1-3 (b) Circuit layout of filter of two λ/4 SIRs with a tapped stub cascaded by three-line coupling structure
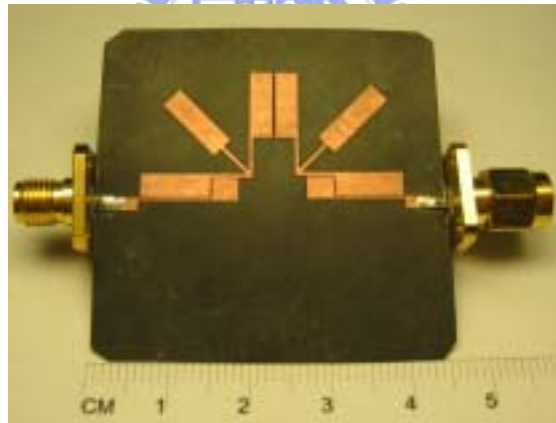
Fig. 3.1-4 (a) Photo of the circuit in Fig 3.1-3 (a)
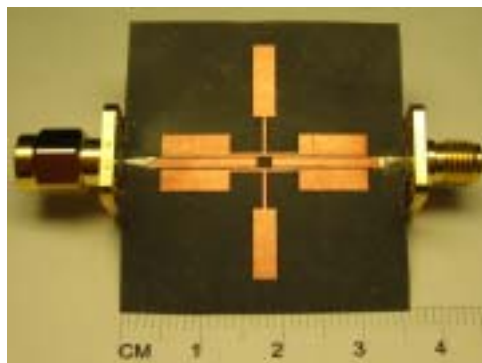
Fig. 3.1-4 (b) Photo of the circuit in Fig 3.1-3 (b)
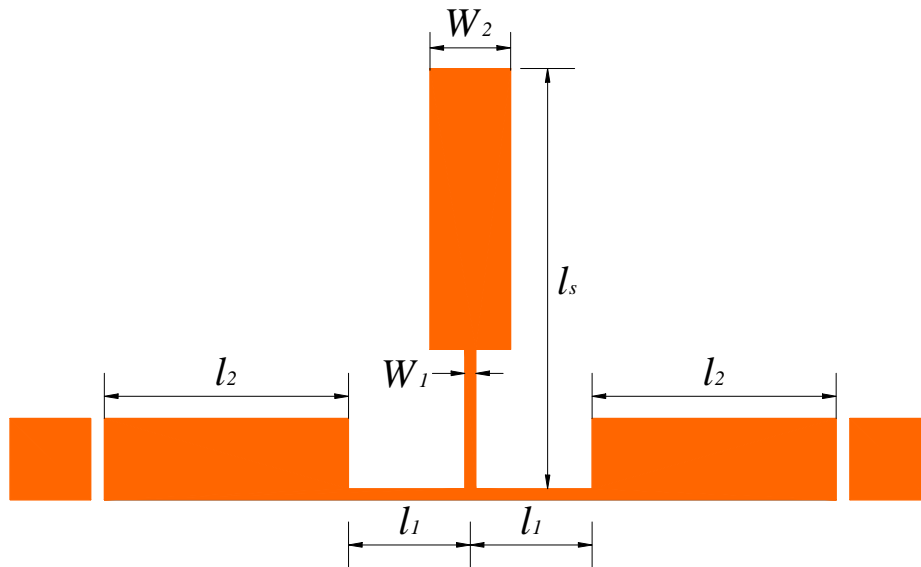
Fig. 3.1-5 (a) Circuit layout of gap-coupling test of two λ/4 SIRs with a tapped stub

Fig. 3.1-5 (b) Dependence of the transmission zero f_z and pole frequencies, f_o and f_p, of the SIR circuit on normalized stub length
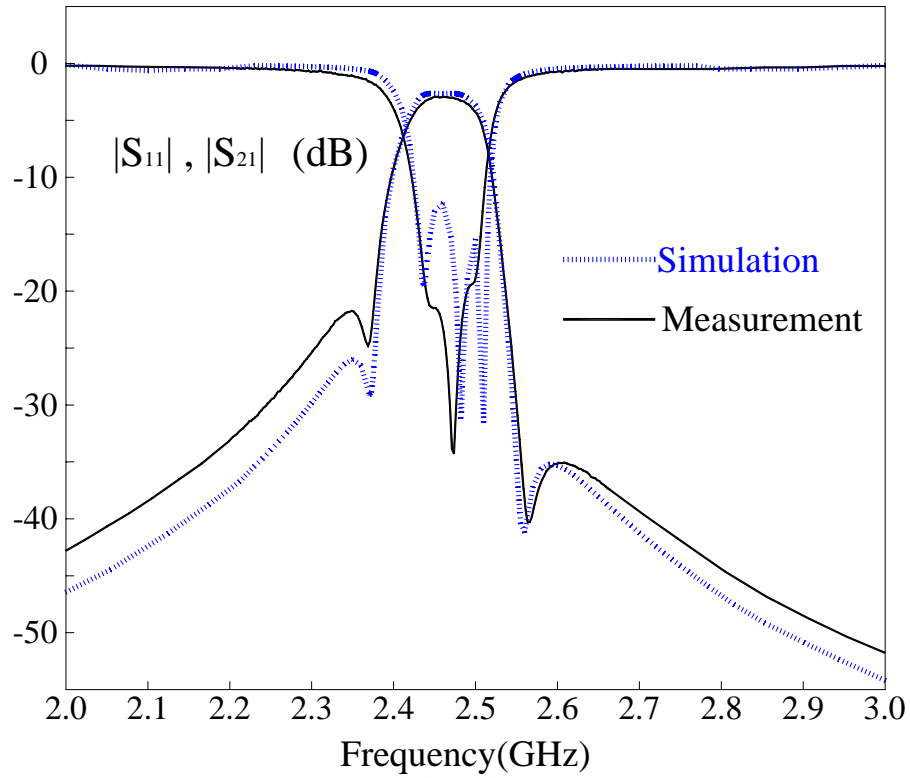
Fig. 3.1-6 (a) Simulation and measurement results of Fig 3.1-3 (a)
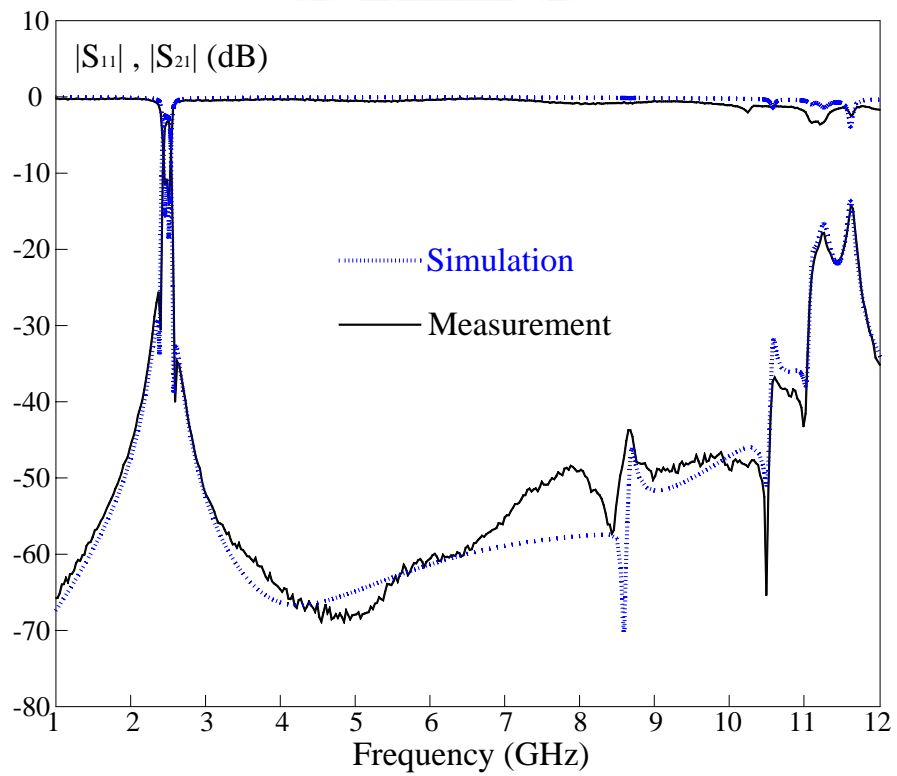
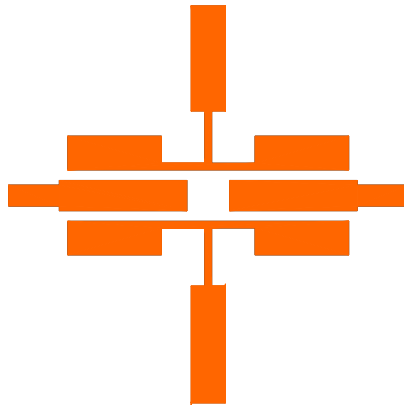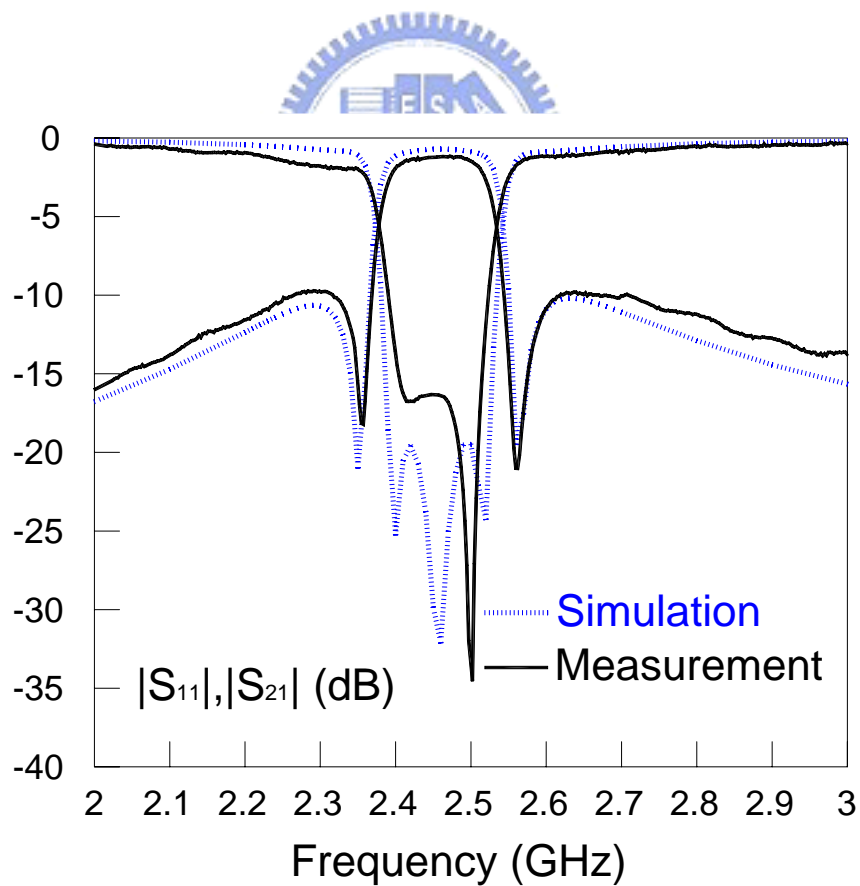Fig. 3.1-6 (b) Broadband simulation and measurement results of Fig 3.1-3 (a)
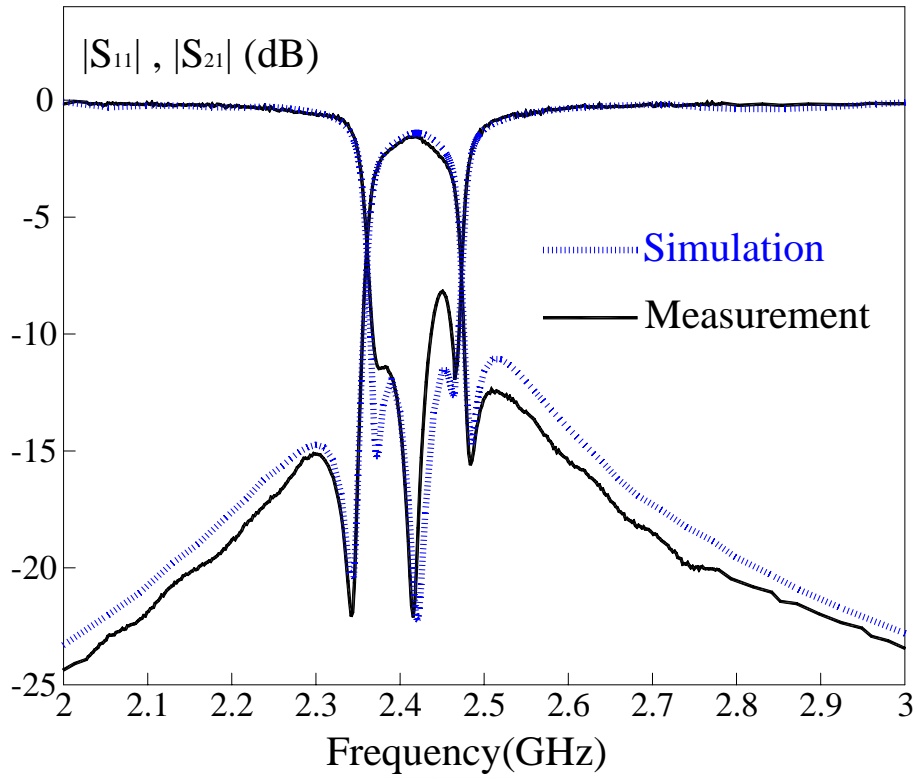
Fig. 3.1-7 (a) Simulation and measurement results of Fig 3.1-3 (b)
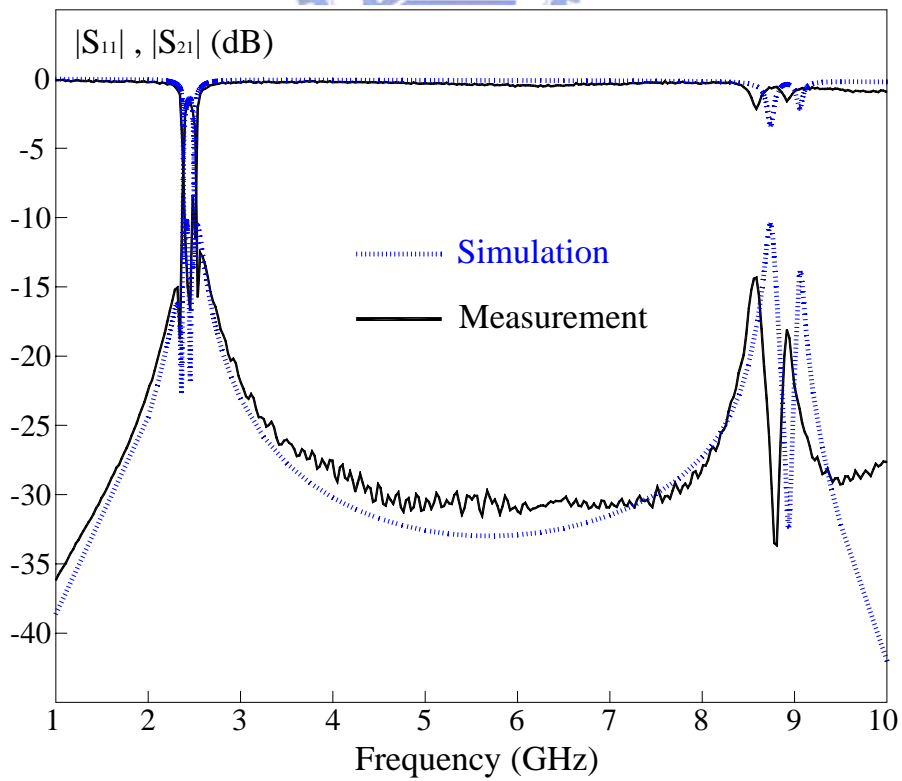
Fig. 3.1-7 (b) Broadband simulation and measurement results of Fig 3.1-3 (b)

Fig. 3.1-8 (a) Circuit layout of filter of two λ/4 SIRs with a tapped stub cascaded by three-line structure on a ε_r = 10.2 substrate of 1.27 mm thickness

Fig. 3.1-8 (b) Simulation and measurement results of Fig. 3.1-8 (a)
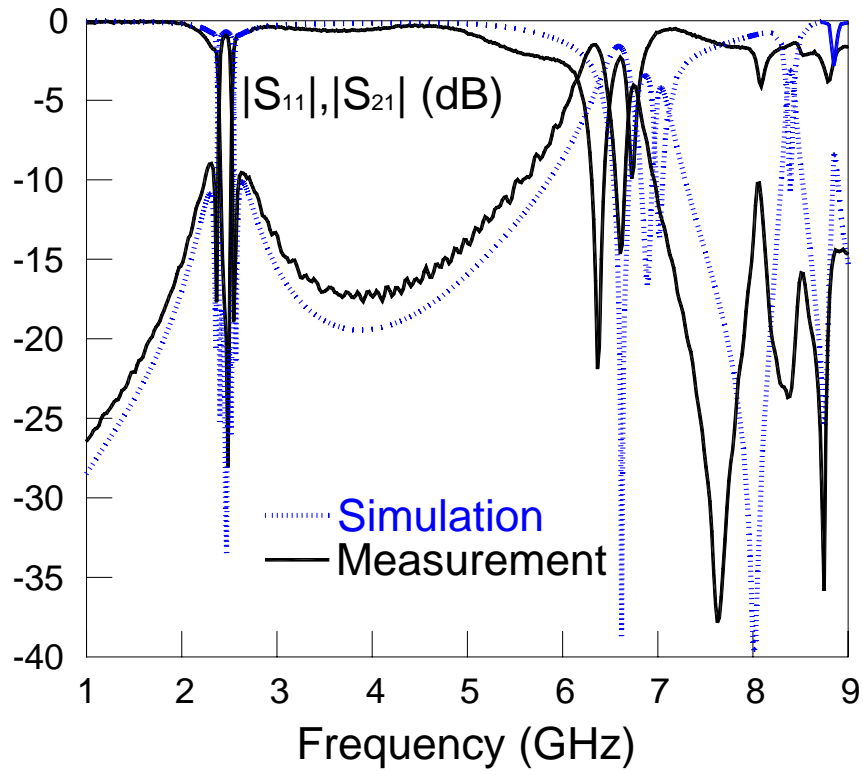
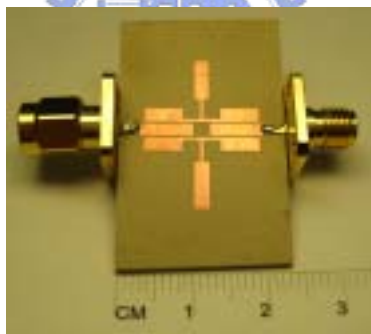Fig. 3.1-8 (c) Broadband simulation and measurement results of Fig. 3.1-8 (a)

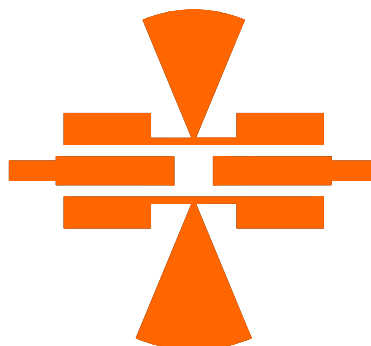Fig. 3.1-8 (d) Photo of the circuit in Fig 3.1-8 (a)

Fig. 3.1-9 (a) Circuit layout of two λ/4 SIRs with a tapped 45° radial stub cascaded by three-line coupling structure on a $\varepsilon_r = 10.2$ substrate of 1.27 mm thickness
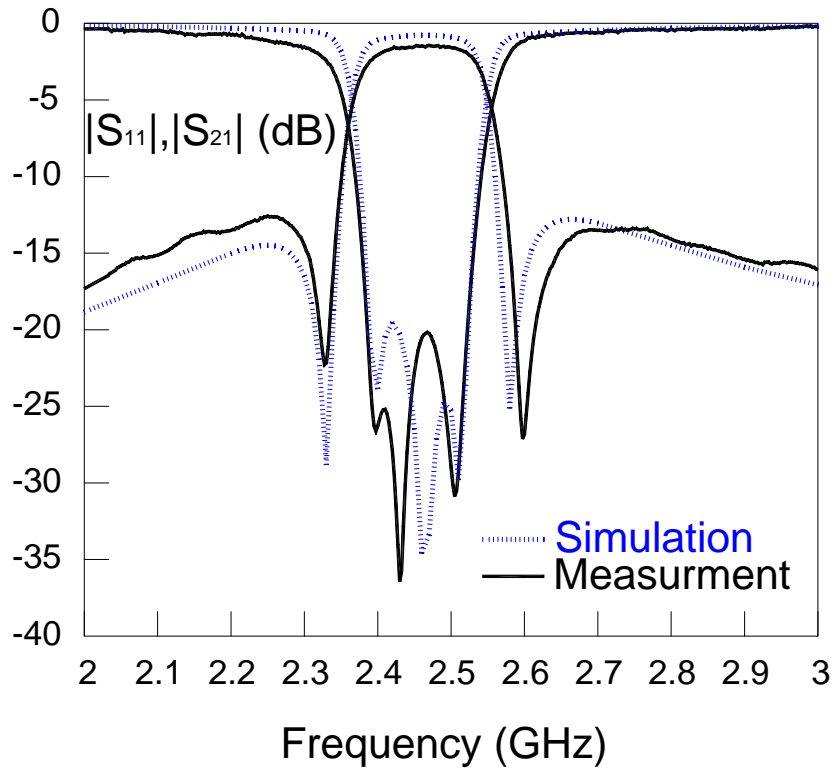
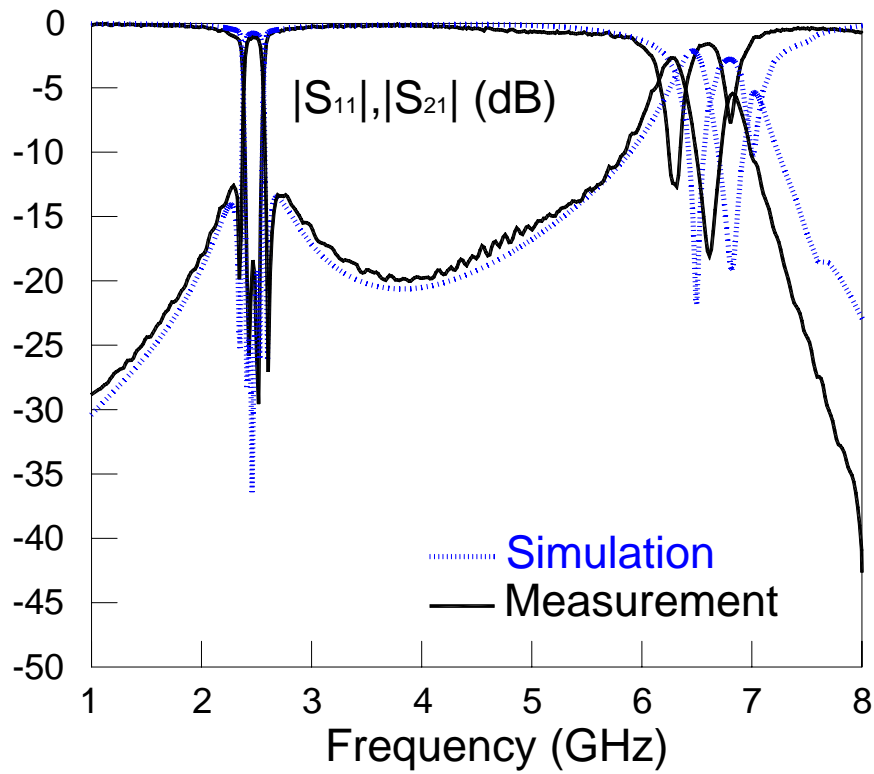Fig. 3.1-9 (b) Simulation and measurement results of Fig. 3.1-4 (a)

Fig. 3.1-9 (c) Broadband simulation and measurement results of Fig. 3.1-4 (a)
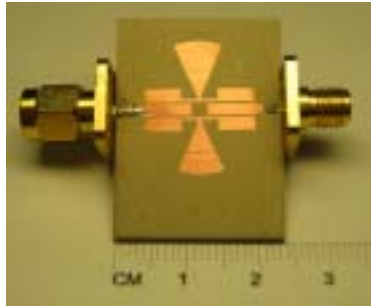
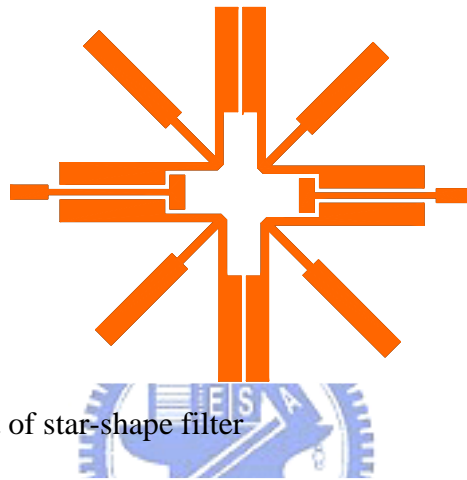Fig. 3.1-9 (d) Photo of the circuit in Fig 3.1-9 (a)

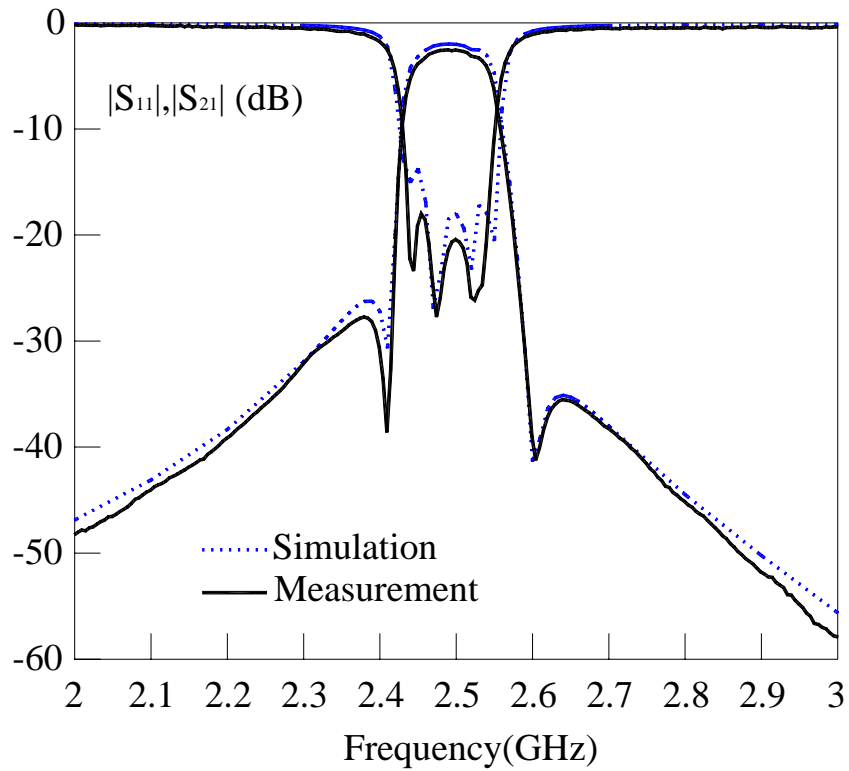Fig. 3.1-10 (a) Circuit layout of star-shape filter

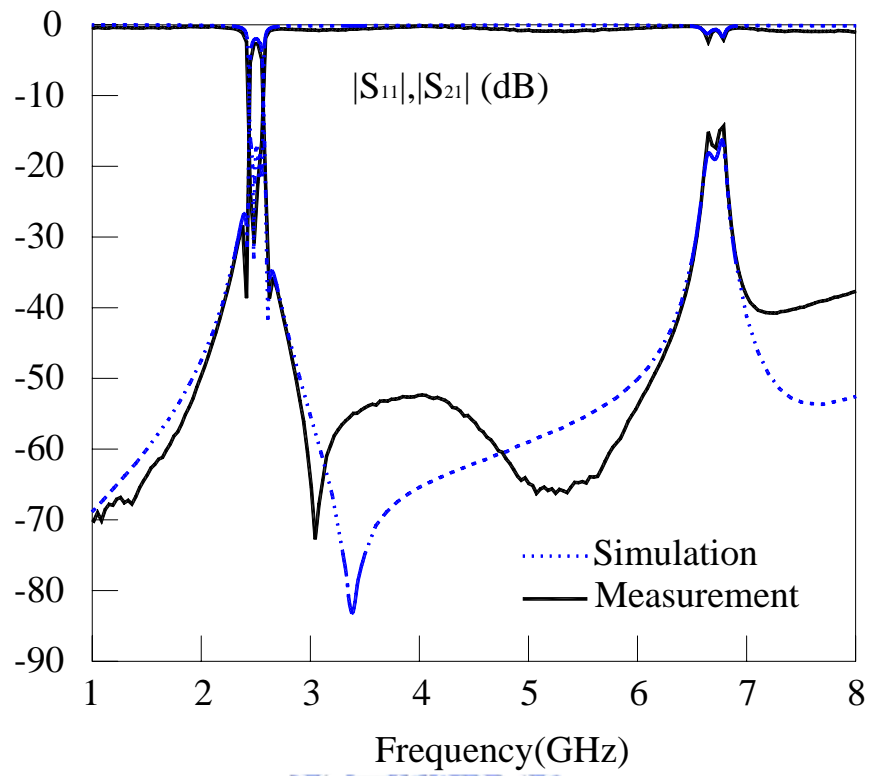Fig. 3.1-10 (b) Simulation and measurement results of Fig. 3.1-10 (a)

Fig. 3.1-10 (c) Broadband simulation and measurement results of Fig. 3.1-10 (a)
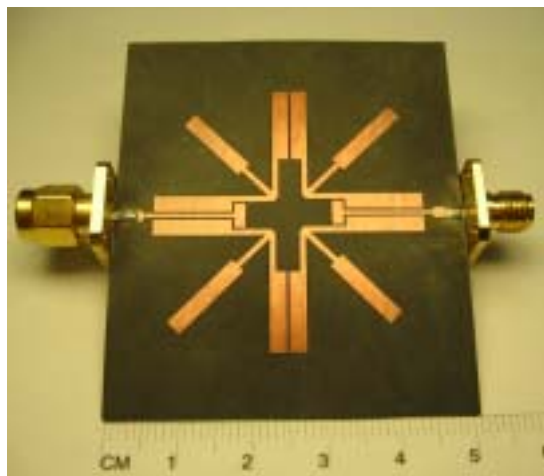

Fig. 3.1-10 (d) Photo of the circuit in Fig 3.1-10 (a)

Chapter 4

Conclusion

A simple design for bandpass filters with a sharp transition is presented. The building blocks of the filters are quarter-wavelength uniform impedance resonators (UIRs) and stepped-impedance resonators (SIRs) with a tapped open stub. Both direct coupling scheme and a three-line coupling structure are used to realize the cascade of two coupled stages. Transmission zeros are created on both sides of the passband. Direct coupling structure can be easily implemented; however it will suffer from realization of the small coupling gap size and the tuning of resonator dimensions while the filter synthesizing. Three-line coupling structure can mainly eliminate the adjustment work and also release the coupling gap size limitation.

The UIR design presents good $|S_{11}|$ responses as well as good insertion loss in the passband, while the SIRs design case possesses a wide upper rejection band with a good attenuation level. All the presented filters show a sharp transition band. In particular, the three-line coupling structure can perform a sharper transition. In addition, several improvement techniques to achieve a flatter passband and better stopband rejection level by exploiting different substrate and radial stubs are presented, while the elliptic function-like responses are still unaltered. The flatter passband response usually conflicts with a poor rejection level, although taking advantage of the radial-type stub will just obtain limited improvement in filter performance. Certain trade-off can be made to meet user's demands.

Reference

[1] J.-S. Hong and M. J. Lancaster, "Couplings of microstrip square open-loop resonators for cross-coupled planar microwave filters," *IEEE Trans. Microwave Theory & Tech.*, vol. 44, no. 11, pp. 2099–2109, Nov. 1996.

[2] J.-T. Kuo, M.-J. Maa and P.-H. Lu, "A microstrip elliptic function filter with compact miniaturized hairpin resonators," *IEEE Microwave and Guided Wave Letters*, vol. 10, no. 3, pp. 94–95, Mar. 2000.

[3] C.-C. Yu and K. Chang, "Novel compact elliptic-function narrow-band bandpass filters using microstrip open-loop resonators with coupled and crossing lines**,"** *IEEE Trans. Microwave Theory & Tech.*, vol. 46, no. 7, pp. 952–958, July 1998.

[4] K. Wada and I. Awai, "Heuristic models of half-wavelength resonator bandpass filter with attenuation poles," *IEE Electronics Letters*, vol. 35, no. 5, pp. 401–402, Mar. 1999.

[5] J.-T. Kuo and E. Shih, "Microstrip stepped impedance resonator bandpass filter with an extended optimal rejection bandwidth," *IEEE Trans. Microwave Theory Tech*., vol. 51, no. 5, pp. 1554-1559, May 2003.

[6] S.-Y. Lee and C.-M. Tsai, "New cross-coupled filter design using improved hairpin resonators," *IEEE Trans. Microwave Theory and Tech*., vol.48, no.12, pp. 2482–2490, Dec. 2000.

[7] J.-R Lee, J.-H. Cho and S.W. Yun, "New compact bandpass filter using microstrip λ/4 resonators with open stub inverter," *IEEE Microwave and Guided Wave Letters*, vol. 10, no. 12, pp. 526–527, Dec. 2000.

[8] J.-T. Kuo and E. Shih, "Wideband bandpass filter design with three-line microstrip structures," 2001 *IEEE MTT-S Int. Microwave Symp. Dig.*, pp.1593-1596, May 2001.

[9] IE3D simulator (Zeland Software Inc., Jan. 1997).

[10] R. SCHWINDT. and C. NGUYEN, " Spectral domain analysis of three symmetric

coupled lines and application to a novel band pass filter," *IEEE Trans. Microwave Theory Tech.*, 1994, 42, (7), pp. 1183-1189.

[11] J.-T. Kuo, "Accurate quasi-TEM spectral domain analysis of single and multiple coupled microstrip lines of arbitrary metallization thickness," *IEEE Trans. Microwave Theory Tech.*, 1995, 43, (8), pp.1881-1888.

[12] F.-L. LIN, C.-W. CHIU, and R.-B. WU, "Coplanar waveguide bandpass filter - a ribbon-of-brick-wall design," *IEEE Trans. Microwave Theory Tech.*, 1995, 43, (7), pp. 1589-1596.

[13] D.M. POZAR, "Microwave Engineering," (John Wiley & Sons, New York, 1998, 2nd edition)

[14] Franco Giannini, Robert Sorrentino, Jan Vrba, "Planar circuit analysis of microstrip radial stub," *IEEE Trans. Microwave Theory Tech.*, vol.32, no.12, pp. 1652-1655, Dec. 1984.

[15] C.-M. Tsai, S.-Y. Lee, H.-M. Lee, "Transmission-line filters with capacitively loaded coupled lines," *IEEE Trans. Microwave Theory Tech.*, vol.51, no.5, pp. 1517-1524, May. 2003.

（Wan-Hsin Hsieh）

68　12　13

(91.9 ~ 93.6)

(87.9 ~ 91.6)

(84.9 ~ 87.6)

1. Jen-Tsai Kuo, Wan-Hsin Hsieh and Meshon Jiang, "Design of Two-Stage UIR and SIR Bandpass Filters with an Elliptic Function-Like Response," to be presented in *2004 IEEE MTT-S International Microwave Symposium Digest*, Fort Worth, Texas, USA, June 6-11, 2004.